We are IntechOpen, the world's leading publisher of Open Access books Built by scientists, for scientists

6,900
Open access books available

185,000
International authors and editors

200M
Downloads

Our authors are among the

154
Countries delivered to

TOP 1%
most cited scientists

12.2%
Contributors from top 500 universities



WEB OF SCIENCE™

Selection of our books indexed in the Book Citation Index in Web of Science™ Core Collection (BKCI)

Interested in publishing with us?
Contact book.department@intechopen.com

Numbers displayed above are based on latest data collected.
For more information visit www.intechopen.com



7

Metal Oxides and Their Composites for the Photoelectrode of Dye Sensitized Solar Cells

Jae-Joon Lee[1], Md. Mahbubur Rahman[2], Subrata Sarker[2], N.C. Deb Nath[2], A.J. Saleh Ahammad[2] and Jae Kwan Lee[3]

[1]*Department of Applied Chemistry, Konkuk University, Chungju 380-701,*
[2]*Department of Advanced Technology Fusion, Konkuk University, Seoul 143-701,*
[3]*Research Center for Convergence Technology, Hoseo University, Chungnam 336-795*
Korea

1. Introduction

Nowadays, solar energy is one of the most promising future energy resources in concerns to the sustenance of life on Earth and the depletion of fossil fuels. It is projected that the fossil fuel related CO_2 emissions rise from 32 to 42 billion metric tons in 2007 and 2035 (EIA., 2010). This enormous amount of CO_2 emission will leads to a severe climatic change of the world and therefore a greatest anxieties for the scientific era of 21st century. This rigorous apprehension leads the scientist for the development of solar cell that utilizes solar energy, a renewable and carbon free energy source. The solar energy strike to the earth in one hour is about 4.3×10^{20} J, which is higher than all the energy consumed in the planet (4.1×10^{20} J). Therefore, covering 0.1% of the earth's surfaces with solar cell of 10% efficiency would satisfy the current energy demand (Grätzel., 2001).

In general, solar cells can be classified as p-n junction semiconductor solar cells and organic-based exitonic solar cells (OESCs), in which polymer solar cell (PSC), dye sensitized solar cell (DSSC) and hybrid solar cell are included. In 1991, O'Regan & Grätzel first reported the dye sensitized nanocrystalline TiO_2 solar cell (DSSC) based on the mechanism of a first regenerative photoelectrochemical processes with an efficiency of 7.1-7.9 %(under simulated solar light) (O'Regan & Grätzel., 1991). Since then, extensive researches have continued to increase the power conversion efficiency (PCE) of DSSC by incorporating n-type metal oxide semiconductors such as TiO_2, ZnO, SnO_2, Nb_2O_5, $SrTiO_3$ etc and their composites as photoelectrode materials to achieve a reasonable efficiency of DSSCs of low cost, being therefore a promising alternative to conventional p-n junction solar cell. The wide band gap (E_g > 3eV) metal oxide semiconductors having suitable band position relative to sensitizer has been employed for the fabrication of DSSCs. The high surface area of nanoporous metal oxides facilitates the improvement of light absorption with improved dye loading for improved performance of DSSC. It is evident that the metal oxides employed for the fabrication of DSSCs has solar absorption below a threshold wavelength, λ_g (where, $\lambda_g = 1240/E_g$), i.e., they have absorption at ultraviolet region. On the other hand, dye is only responsible for the absorption of light at visible and near-infrared region. The strong absorption of light is attributed to the intramolecular charge transfer transition (ICT) from electron donating group to the anchoring acceptor group of dye. Therefore, the anchored

dye on to the metal-oxide surface helps the red shift of absorption threshold of metal oxide near infrared region (Rengaraj et al., 2005). In addition to the above physical characteristics, the inexpensiveness, natural abundancy and facile synthesis methods of metal oxides and their composites is another advantage for the application in DSSCs.

This chapter discusses the understanding the fundamental of DSSCs, different structural and technical aspect of metal oxides and their composites for the stepwise development of the performance of DSSCs. In addition, we focuses on the understanding of interfaces between metal oxides (or metal oxide composites)/dye/electrolyte, in which the electron injection and transport for improving the efficiency of DSSCs are related. Figure 1 represents the energy band diagram vs. vacuum of the metal oxides describes in this chapter.

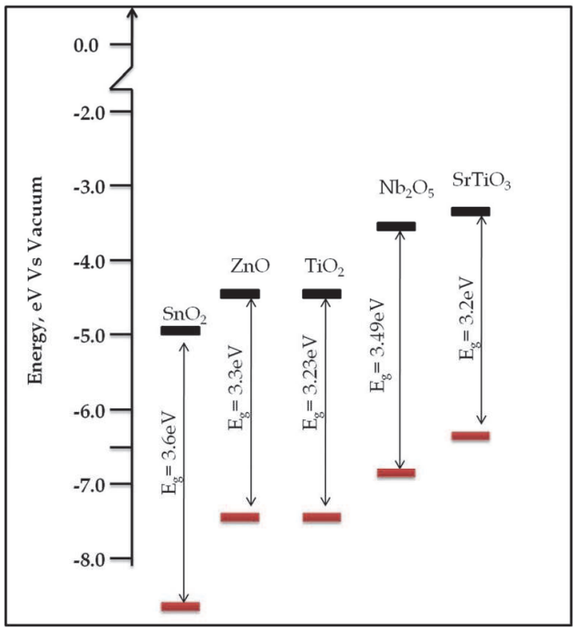


Fig. 1. Energy band diagram of the representative metal oxides applied in DSSC (vs vacuum). The lower edge of the conduction band (CB) (black) and the upper edge of the valence band (VB) (red) are presents along with the band gap in electron volts (eV). Energy levels were taken from the following references (Grätzel., 2001; Wei et al., 2008; Hod et al., 2010)

2. Dye sensitized solar cell (DSSC)

Figure 2 shows a schematic representation of the operating principle of DSSC. Based on the electron transfer mechanism from dye to TiO_2 conduction band, DSSC can be classified into two distinct classes: Type-I, and type-II. The heart of the system is mesoporous semiconducting metal oxide (mostly employed TiO_2) film that is placed in contact of a redox electrolyte (such as I^-/I_3^-, Br^-/Br_2, $SCN^-/(SCN)_2$, $SeCN^-/(SeCN)_2$, bipyridine cobalt (III/II) complexes) (Wang et al., 2005; Nusbaumer et al., 2001; Wang et al., 2004; Sapp et al., 2002; Bergeron et al., 2005) or a hole conductor (such as CuI, CuBr, CuSCN, spiro-MeOTAD) (Wu et al., 2008). A monolayer of the sensitizer (typically bipyridine ruthenium complexes) such as *cis*-diisothiocyanato-bis(2,2′-bipyridyl-4,4′-dicarboxylato)ruthenium(II) bis(tetrabutylammonium) (N719), *cis*-bis(isothiocyanato)bis(2,2'-bipyridyl-4,4'-dicarboxylato)-ruthenium(II) (N3), and *cis*-disothiocyanato-(2,2′-bipyridyl-4,4′-dicarboxylic

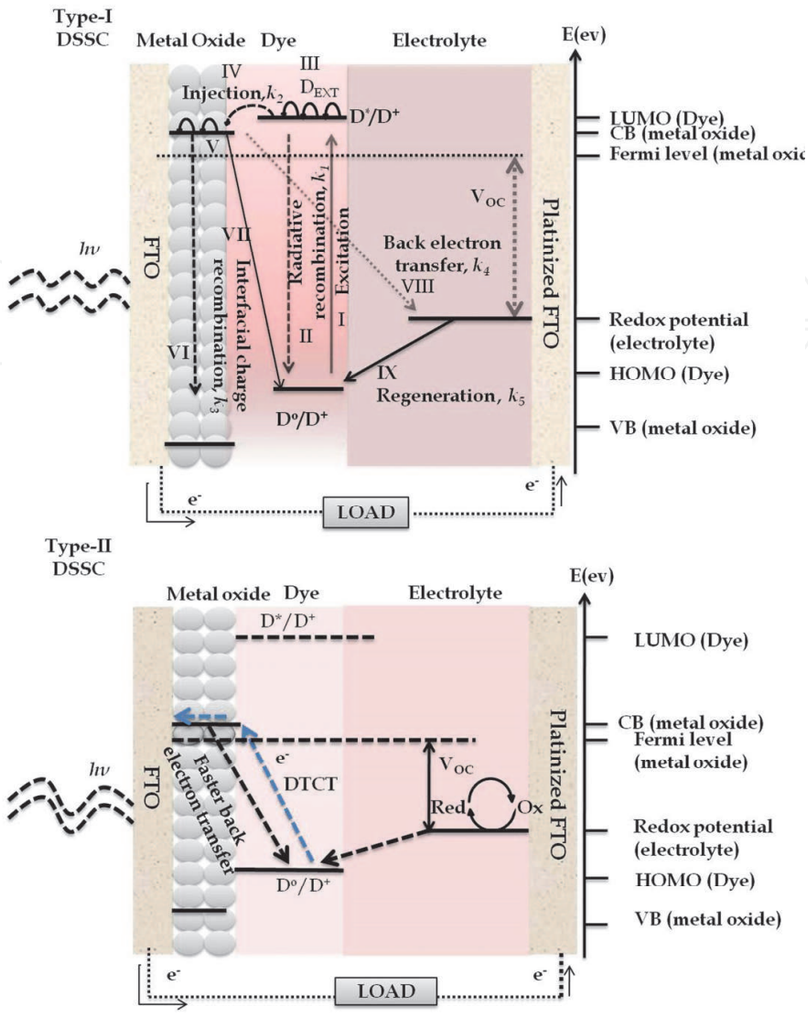


Fig. 2. Principle of operation of type-I & type-II dye sensitized solar cell (DSSC)

acid)-(2,2′-bipyridyl-4,4′-dinonyl)ruthenium(II) (Z907) etc is attached to the surface of the nanocrystalline metal oxide film in type-I DSSC (Thavasi et al., 2009). The type-I DSSC is understood as general electron transport mechanism, where the photoexcitation of dye results the injection of electron to the conduction band (CB) of the metal oxides from the excited dye, i.e. from the LUMO level. On the other hand, in type-II DSSCs, enediol group, catechol and its derivatives such as dopamine, fluorone, and anthocyanins having catechol moieties gives strong direct dye-to-metal-oxide (TiO_2) charge transfer (DTCT) bands. Therefore, electrons are injected directly from HOMO of dye to the conduction band (CB) of metal oxide rather than from the excited state (LUMO) under illumination (i.e. one-step electron injection) (Tae et al., 2005). A platinized cathode is employed to collect the electrons from the conduction band of metal oxide anode injected from the excited dye and to catalyze the redox couple *viz.* I^-/I_3^- regeneration reaction. The redox couple of the electrolyte also reduces the oxidized dye. The iodide regenerated, in turn, by the reduction of triiodide at the cathode, with the circuit being completed via electron movement through the external load. The voltage generated under illumination is the difference between the Fermi level of the electron in metal oxide and the redox potential of the electrolyte. Overall, the device

generated electric power from sunlight without suffering any enduring chemical conversion (Grätzel., 2003; Bisquert et al., 2004). Whereas, in type-II DSSC faster back electron transfer limit its conversion efficiency, over and above commercial application (Huber et al., 2000; Wang et al., 2003). In this chapter, the application of metal oxide and their composites is mainly focused in type-I DSSC.

2.1 Photochemical processes in DSSCs and rate limiting steps

The photoelectrochemical process in DSSC can be expressed by the following reaction a-f. Where, electron injection (reaction b) of the photoexcited dye to the conduction band (CB) of metal-oxide (TiO_2) occurs in subpicosecond range (200 fs for coumarin dye to TiO_2) (Hara et al., 2000). Reaction (c) and (d) represents the regeneration of photoexcited dye by the oxidation of I^- to I_3^- and the reduction of I_3^- to I^- by Pt catalyst at cathode respectively. Reaction (e) and (f) correspond to the dark reaction occur during the photoconversion and do not play a significant negative impact on the photovoltaic performance of DSSC due to their sluggish reaction rate compared to the reaction (b).

Metal oxide (TiO_2) | D+hv	→ Metal oxide (TiO_2) | D*	excitation	(a)
Metal oxide (TiO_2)| D*	→ Metal oxide (TiO_2) | $D^+ + e^-_{(CB)}$	injection	(b)
Metal oxide (TiO_2)| $D^+ + 3I^-$	→ Metal oxide (TiO2) | $D + I_3^-$	regeneration	(c)
$I_3^- + 2e^-_{(Pt)}$	→ $3I^-$	reduction	(d)
$I_3^- + 2e^-_{(CB)}$	→ $3I^-$	reception (dark reaction)	(e)
Metal oxide (TiO_2)| $D^+ + e^-_{(CB)}$	→ Metal oxide (TiO_2)| D	recombination (dark reaction)	(f)

Photovoltaic performance is significantly influenced by the events in interfaces between the metal oxide semiconductor, the dye, and the electrolyte. The dye/metal oxide interface is such that the oxidation potential of excited dye (LUMO) is sufficiently negative to obtain the effective electron injection to the conduction band of metal oxide. Upon photoirradiation, dye molecule undergoes a $\pi \rightarrow \pi^*$ transition thereby exciting an electron to the LUMO due to the relatively weak lateral overlapping of atomic orbital's (π bonds) with loosely bound electrons (π electrons) in HOMO. These excited electrons diffuse into the dye/metal oxide interface. Hence, a built in energy gradient (ΔE) exists between the dye/metal oxide interface due to the energy difference between the LUMO state of dye and the CB of metal oxide (E_{CB}). Thus, electrons in the LUMO of photoexcited dye undergo a nonradiative transition to the conduction band of metal oxide within a few picoseconds and thereby oxidized. The oxidized dye is reduced back to its ground state by using a redox couple together with platinum as catalyst at cathode (Thavasi et al., 2000; Jose et al., 2009).

The fundamental phenomenon of photoconversion and rate limiting steps involved in DSSCs (type-I) depicted in figure 2 are listed below:

I. The rate of excitation of dye: it is determined by the absorption of the number of photon at the absorption wavelength of dye, intensity of solar radiation at that window, and the absorption cross-section of dye.
II. The relaxation/radiative recombination of the excited electron of dye from LUMO to HOMO, and the corresponding rate constant k_1: Relaxation processes occur typically in a time scale of nanoseconds. This process reduces the excited state free energy by ~ 400 meV. The typical rate of excited state decay to ground state of dye is in the range 10^7-10^{10} s^{-1} (Grätzel & Durrant., 2008).
III. Exciton diffusion length D_{EXT}.

IV. Interfacial electron transfer, i.e., the injection of excited electron from the LUMO of dye to the conduction band of metal oxide with the rate constant k_2: The kinetics of the interfacial electron transfer dynamics strongly depends on the energetic of metal oxide/dye/electrolyte interface and the density of electron in metal oxide (*i.e.* the Fermi level of metal-oxide). The interfacial charge transfer occurs in a time scale of several picoseconds. In model system studies of dye sensitized metal oxide films, electron injection rate of > 10^{12} s^{-1} have reported for a range of sensitizer (Grätzel & Durrant., 2008).
V. Injected electron transport through the mesoporous layer of metal oxide to the transparent conducting oxide (TCO). It is controlled by the diffusion coefficient of electron (D_e), and the electron lifetime (τ_e).
VI. Phonon relaxation, through which an electron loses its energy by electron-phonon recombination.
VII. Interfacial charge recombination, i.e., the capturing of electron from the conduction band (CB) of metal oxide by the oxidized dye with the rate constant k_3: Charge recombination occurred from the CB of photoelectrode to oxidized dye in the range of μs-ms. This recombination rate is strongly depends on the electron density of the photoelectrode, light intensity, and cell voltage.
VIII. Back electron transfer, i.e., the capturing of CB electrons by the oxidized mediator in the electrolyte (e.g. I_3^-) with the rate constant k_4: Back electron transfer typically very slow (in the range of ms-s) and the rate constant is strongly dependent on the concentration and viscosity of the electrolytes as well as the structure of dye (Grätzel & Durrant., 2008).
IX. Regeneration of dye, i.e., the transfer of electron to the oxidized dye from the redox mediator in the electrolyte with the rate constant k_5: The restoration of the oxidized dye takes place in the nanosecond range. It is typically 100 times quicker than any recombination reaction and about 108 times faster than the inherent lifetime of the oxidized dye (Grätzel & Durrant., 2008).

In case of N719 dye, the interfacial charge recombination and the regeneration rate constants are k_3 = 1.4x10^3 s^{-1} and k_5 = 1.1x10^5 s^{-1}, respectively. This implies the injection yield of 99%, since the regeneration step is ~100 times faster than recombination. Also, the rate of the injection of electron (k_2 > 1.4 X 10^{11} s^{-1}) is three order of magnitude faster than the radiative recombination (Grätzel & Durrant., 2008). Consequently, it is assumed that interfacial charge recombination and radiative recombination, the two rate limiting processes, do not limit significantly the photoconversion of DSSCs. In addition, the exciton diffusion could be neglected since the exciton is highly localized on dyes because the particle radius is significantly smaller than the Bohr radius. Thus, the rate limiting processes that contribute highly on the photoconversion efficiency are (I), (IV), (V), (VI), (VIII) and (IX). The rate limiting steps, (I) and (IX) are dependent on the dyes and electrolyte, respectively. Steps (IV) and (VIII) depend on the interface between metal oxide/dye and metal oxide/electrolyte interface. The other two steps, (V) and (VI), are completely depends on photoelectrode (Jose et al., 2009). It is clear that the metal oxides, one of the major constituent of the photoelectrode, play a significant role on the performance of DSSCs by involving with most of the operation processes in the DSSCs.

2.2 Characterization techniques of DSSCs

Photoelectric current-voltage (I-V) measurement, electrochemical impedance spectroscopic measurement (EIS), and incident photon to current conversion efficiency (IPCE) measurements are the major essential techniques for the characterization of DSSCs.

2.2.1 Photoelectric current-voltage (I-V)

The photovoltaic performance of DSSCs is estimated from the current-voltage (I-V) measurements. The photovoltaic parameters of DSSCs are open circuit potential (V_{oc}), short circuit current (I_{sc}), fill factor (FF), and efficiency (η). These parameters are measured under the standard condition of cell temperature 25 ^{0}C, incident solar radiation of 100 mW/cm^2, and the spectral power distribution of AM1.5. Figure 3A depicts the I-V characteristics of a DSSCs made with N719 sensitized TiO_2 (degusa P25) photoelectrode of active area 0.2 cm^2 (Figure 3B). It is assumed that the standard redox potential of electrolyte is constant and, therefore, the V_{oc} of a phototelectrochemical cell should also constant. However, the V_{oc} of a photoelectrochemical cell can be control by tuning the flat band (V_{FB}) of metal oxide with introducing metal oxide composites or dopants into metal oxides (Lü et al., 2010).

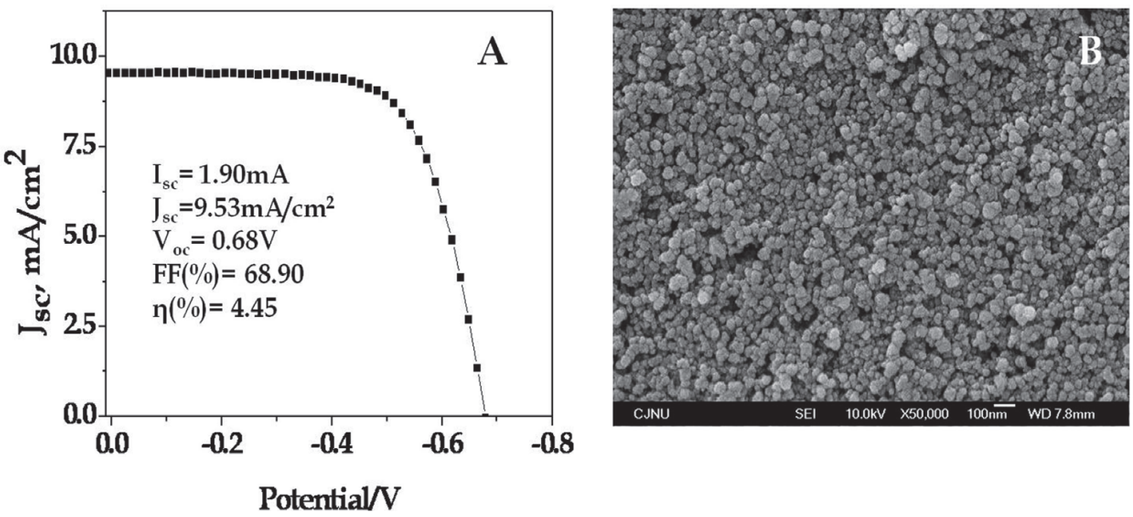


Fig. 3. (A) Photovoltaic performance of a state-of-the-art DSSC laboratory cell: *I–V* curve measured under AM 1.5 standard test conditions and (B) Scanning electron micrograph (SEM) of a sintered mesoporous TiO_2 (Degusa P25) film supported on FTO

Short circuit current density (J_{sc}) is the photocurrent per unit active area (A) of the photoelectrode when the applied potential across the DSSCs is zero, i.e. $J_{sc} = I_{sc}/A$. Under the ideal illumination condition, J_{sc} is effectively dependent on the efficiency of charge injection from the excited dye to the CB of metal oxide. The electron injection efficiency of some widely used metal oxides is found to be the following order: TiO_2 > Nb_2O_5 > SnO_2~ZnO (Thavasi et al., 2009).

Fill factor (*FF*) is the most important parameters of a photovoltaic cell. It is defined as the ratios of maximum power output ($I_{max}xV_{max}$) and the product of V_{oc} and I_{sc}. Therefore, from figure 4,

$$FF(\%) = \frac{I_{max}xV_{max}}{I_{sc}xV_{oc}} = \frac{AreaA}{AreaB} \quad (1)$$

It can be concluded that the more square like I-V curve is essential for highly desired FF. The lowering of electron loss between the FTO/electrolyte interface increases the shunt resistance, thereby increases the fill factor. On the other hand, increase of the back electron transfer and

charge recombination is responsible for poor FF. Finally, comparing the ratios of total power out put (P_{out}) with the solar power input (P_{in}), efficiency (η) can be measured. i.e.,

$$\eta = \frac{P_{out}}{P_{in}} = \frac{J_{sc} V_{oc} FF}{P_{in}} \tag{2}$$

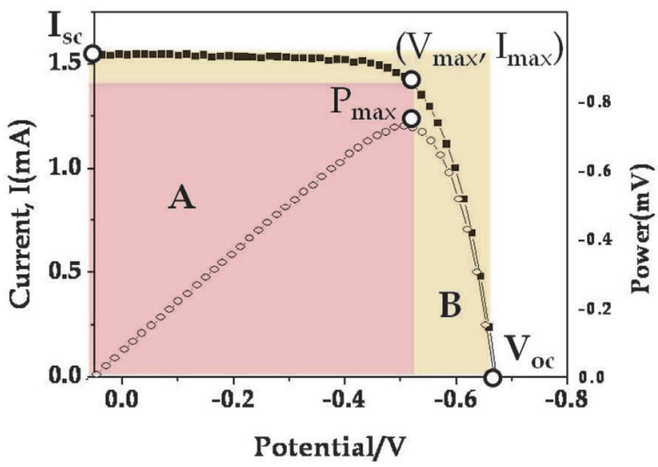


Fig. 4. I-V curve and parameters of DSSCs output current (solid line) and power (blank line) as function of voltage

2.2.2 Electrochemical Impedance Spectroscopy (EIS)

For better understanding the electron transport kinetics in DSSCs, EIS is the most powerful tools. EIS is a steady state process for evaluating the current response to the application of an ac voltage as function of frequency. EIS has been broadly employed to investigate the kinetics of electrochemical and photoelectrochemical processes including the clarification of salient ionic and electronic processes occurring in the DSSCs.

Figure 5 depicts a characteristics impedance spectrum (Nyquist plot) along with the electrical transmission line model of equivalent circuit for DSSC. The transmission line model is purely a combination of resistance (R) and capacitance (C). The series resistance, together with the sheet resistance of fluorine-doped tin oxide (FTO) glass and the contact resistance of the cell is denoted by R_S. R_{CO} and C_{CO} are the series resistance and the capacitance of the FTO/metal oxide interface, respectively. R_{TCO} and C_{TCO} are the charge transfer resistance and subsequent double layer capacitance of the FTO/electrolyte interface respectively. The transport resistance in the metal oxide film is represented by r_t. The charge transfer resistance and the charge recombination processes between electrons in the metal oxide phototelectrode and electrolyte is determined by r_{CT}. C_μ is the chemical capacitance of the metal oxide film. Z_d is the Warburg diffusion of ions in the electrolyte. Finally, R_{Pt} and C_{Pt} are the charge transfer resistance and the double layer capacitance of the platinized FTO counter electrode respectively. Therefore, the steady state process of electron transport resistance through metal oxide film, ion diffusion through electrolyte, chemical capacitance at interface of the metal oxide/electrolyte, double layer charge transfer capacitance at interface of the FTO/electrolyte, and the platinized FTO counter electrode, can be estimate by using this method (Fabregat-Santiago et al., 2007).

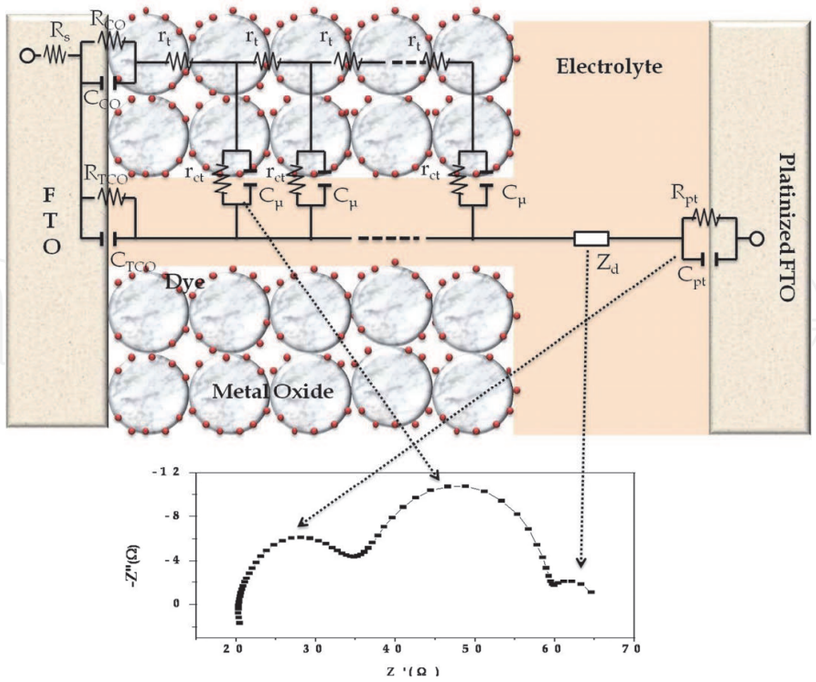


Fig. 5. Typical impedance spectra of DSSCs (Nyquist plot) and its electrical transmission line model of equivalent circuit (The transmission line model is redrawn with permission from ref. Fabregat-Santiago et al., 2007. Copyright 2010, The American Chemical Society)

2.2.3 Incident proton to current conversion efficiency (η_{IPCE})

IPCE is the measurements of spectral response of the cell that contain the partial information of quantum efficiencies of photocurrent generation processes such as the light harvesting (η_{LH}), electron injection (η_{INJ}), and charge collection efficiency (η_{COL}). Therefore,

$$\eta_{IPCE}(\lambda) = \frac{J_{SC}(\lambda)}{q\phi(\lambda)} = \eta_{LH}(\lambda)\eta_{INJ}(\lambda)\eta_{COL}(\lambda) \quad (3)$$

Where, J_{sc} is the short circuit current density of the DSSCs at incident monochromatic light with incident wavelength λ. q and φ is the elementary charge and photon flux respectively (Gentilini et al., 2010). Following each step of conversion, η_{LH} is associated with the ability of the dye in absorbing photons. η_{INJ} quantifies the charge transfer from the LUMO of dye molecule to the conduction band of metal oxide. Finally, the collection efficiency η_{COL} is the amount of electrons that effectively reach the anode, avoiding recombination. It should be noted that IPCE measurement is performed under short circuit condition, where electron lifetime is higher. It is noteworthy that the high fraction of incident photon to current conversion (IPCE) is most important for efficient DSSCs and the mesoporous metal oxide with high surface area is the prerequisite for higher IPCE value.

3. DSSC photoelectrodes with different metal oxides and their composite

As mentioned above, the different metal oxides and their composites have been investigated for the fabrication of DSSC. Herein, some of the important and highly explored metal oxides and their composites as DSSCs photoelectrode will be discussed.

3.1 Titania (TiO_2) / titania composite based photoelectrodes

Nature has abundantly the titanium dioxide (TiO_2) which is relatively inexpensive, and nontoxic. From the time of invention of its photocatalytic activity by Fujishima and Honda in 1972 (Fujishima & Honda.,1972), it has been used in a wide range of application such as paint, pigment, water splitting, hydrogen and oxygen gas sensor, polluting gas sensor, and biosensors (Rahman et al., 2010). The n-type semiconductor TiO_2 has been existed naturally as three crystalline polymorphs, explicitly anatase, rutile, and brookite as shown in figure 6. The crystalline characteristics along with the band gap of TiO_2 ploymorphs has been tabulated in table 1.

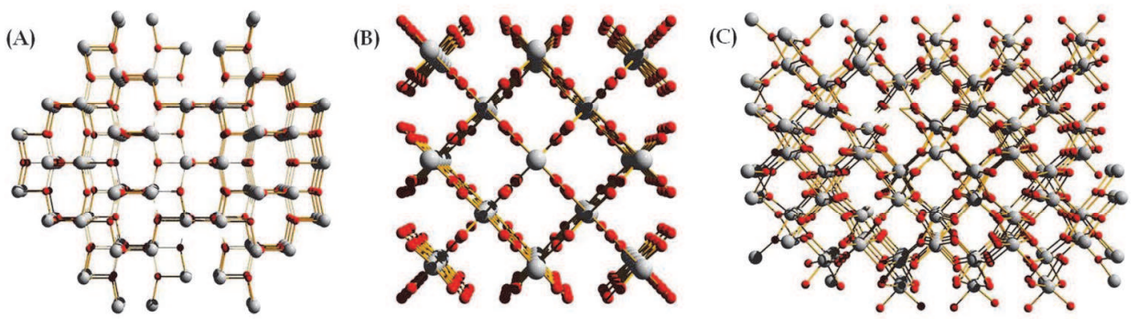


Fig. 6. Different naturally occurs crystalline polymorph of TiO_2 (A) anatase, (B) rutile, (c) brookite, where small red sphere: O^{2-}, big grey sphere: Ti^{4+}

Polymorphs	Band gap	Space group	Cell parameter (Å)	Crystal structure
Anatase	3.23 eV	*I 4₁/amd*	a= 3.7845, c=9.5143	Tetragonal
Rutile	3.05 eV	*P 4₂/mnm*	a= 4.5937, c= 2.9587	Tetragonal
Brookite	3.26 eV	*P bca*	a= 9.1840, b= 5.4470, c= 5.1450	Orthorhombic

Table 1. Crystal characteristics of different TiO_2 polymorphs along with their band gap

In addition, TiO_2 exists in many other metastable forms such as monoclinic, tetragonal, orthorhombic, and cubic. The electronic state of Ti in TiO_2 is Ti^{4+} ($3d^0$), in which the valence band of TiO_2 is composed of the hybridized *2p* orbital of oxygen and the *3d* orbital of Ti, while the conduction band is completely composed of pure *3d* orbital of Ti. Hence, the different parity of valence band and the conduction band of TiO_2 decreases the transition of electrons to the valence band; consequently, decrease the electron hole (e^--h^+) recombination probability. Among the polymorphs of TiO_2, it has known that rutile is the most stable and common. However, the Fermi level of anatase is 100 mV higher than that of rutile, which leads to higher open circuit potential (V_{oc}). Moreover, the greater surface area of anatase is responsible for efficient dye loading, leads the higher photocurrent, consequently, higher photovoltaic performance. Brookite is less prominent for DSSC due to its complicated and difficult synthesis process. It is noted that the oxygen vacancies and the titanium interstitials as well as the decreased recombination probability with increased surface area makes TiO_2 an attractive materials for the application in DSSCs (Li et al., 2007; Jose et al., 2009).

3.1.1 TiO_2 Photoelectrode with passivation layer and 1-D nanostructures

TiO_2 of anatase nanocrystalline form has been explored extensively in DSSCs photoelectrode due to its suitable band position, high surface area for improved dye loading, and facile synthesis procedure. However, the lack of efficient electron transfer through the FTO/TiO_2 interface increases the back electron transfer to the redox ion in electrolyte (Figure 7A) and low light harvesting with low absorption in red region limits the conversion efficiency of DSSCs. Moreover, the random electron diffusion (i.e. electron trapping) and the enhanced grain boundary density of spherical TiO_2 nanoparticles (Figure 7C) increase the loss of conversion efficiency with the increase of carrier recombination (Benkstein et al., 2003). Therefore, extensive efforts have been performed to minimize the back electron transfer/recombination. For example the carrier leakage of direct electron acceptance from the nanocrystalline TiO_2 film can be avoided through prevention of hole mediation to excited dye by addition of 4-tert-butylpyridine into redox solution (Hattori &Goto, 2007). Other impressive ways are the use of TiO_2 passivating layer/blocking layer by using rutile TiO_2 mixed with anatase TiO_2, and the fabrication of DSSCs by one dimensional (1-D) nanostructures such as nanotube, nanowire, nanorod etc(Zhu et al., 2006) .

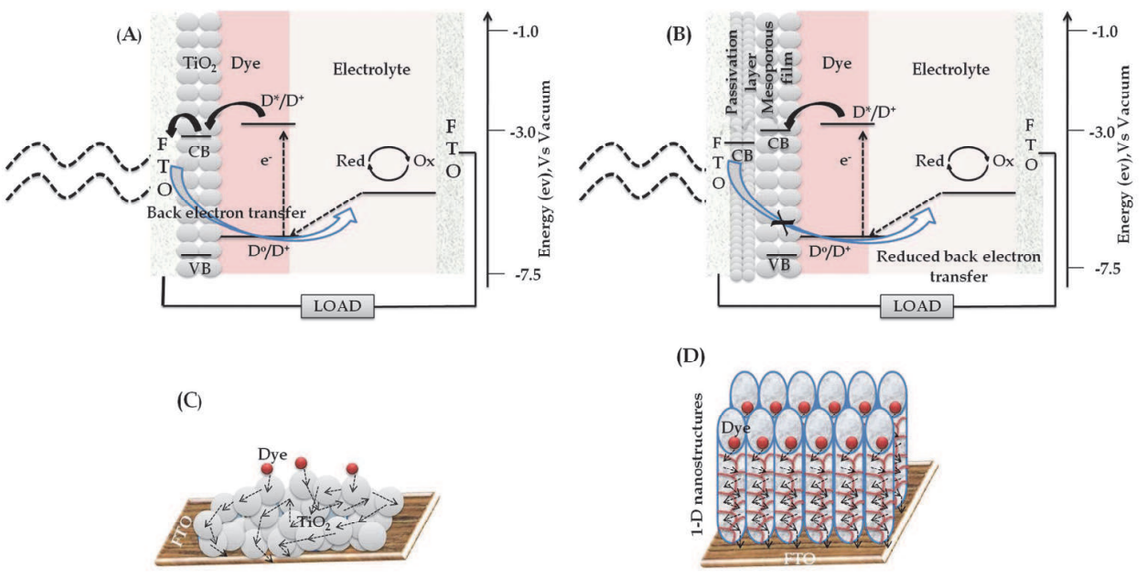


Fig. 7. Schematic representation of spherical anatase TiO_2 nanoparticles based DSSCs, where back electron transfer/recombination is the major role for loss of conversion efficiency (A), photoelectrode with lower passivation layer and upper anatase mesoporous TiO_2 to minimize the back electron transfer (B), random electron diffusion through spherical TiO_2 nanoparticles (C), and 1-D nanostructures of TiO_2 with directional electron diffusion (D)

The important routes of the back electron transfer to electrolyte are to via nanocrystalline TiO_2 and via TCO substrate. However, the back transfer from FTO to the I^-/I_3^- redox couple is negligible because the Fermi level of FTO is close to the redox Fermi level at open circuit potential. Thus, the direct route of recombination of I^-/I_3^- redox couple is to via the nanocrystalline TiO_2. Many researches are focused to prevent this back electron transfer by using a lower passivating layer (rutile/rutile mixed TiO_2) with an upper layer of mesoporous

anatase TiO_2 film. The compact TiO_2 layer not only act as a shielding layer against the ionic penetration but also provoke different microstructure in the sol-gel derived TiO_2 electrodes, which in turn leads to different amount of dye absorption (Yu et al., 2009). All the DSSCs with passivating layer shows higher efficiency than that of without passivating layer. The increase of J_{SC} is generally related to the enhancement of the number of photogenerated electrons that efficiently transferred to TiO_2 electrode. The TiO_2 passivating layer has both of rutile and anatase phases (3.05 eV <Eg> 3.23 eV) and the upper mesoporuos TiO_2 film has only anatase phase (Eg = 3.23 eV). So, the injected excited electrons move in the direction of lower energy conduction band from the porous TiO_2 to the passivating layer, thus resulting in a smooth electron movement and reduce the back electron transfer (Figure 7B). In Table 2, we tabulate the comparison performance of DSSCs before and after using TiO_2 (rutile) passivating layer along with the deposition techniques of passivation layer and mesoporous layer.

Materials	Deposition techniques of passivation layer	Process for making mesoporous TiO_2 layer	Efficiency with (without) passivation layer	Ref.
A thin passivating TiO_2 (rutile) underlayer	Facing target sputtering (FTS) method	Sol-gel	2.85% (0.79%)	Hossain et al., 2008
A thin passivating TiO_2 (rutile) underlayer	Sputtering method	Sol-gel	5.25% (3.85%)	Hattori & Goto, 2007
A thin compact TiO_2 (rutile)layer	Dip-coating	Sol-gel	7.6% (5.7%)	Yu et al., 2009

Table 2. Performance of DSSCs after using passivating layer and their deposition process

Another important technical phase for the improvement of performance of DSSCs is to use 1-D TiO_2 nanostructures. Figure 7D shows the 1-D nanostructures and their directional electron diffusion. Frank and coworkers investigated the comparative study of electron transport and recombination in DSSCs between TiO_2 nanotubes (TNTs) and spherical nanoparticles (NPs) by frequency-resolved modulated photocurrent/photovoltage spectroscopy (Zhu et al., 2006). The rate of recombination in TNTs photoelctrode is much slower than that of NPs photoelectrode. This increase the charge collection efficiency in TNTs photoelectrode compare to NPs photoelectrode. The internal and external dye loading with stronger internal light-scattering effects of TNTs exhibits higher photoconversion efficiency. However, the dye loading of TNTs and charge collection efficiency is strongly dependent on the nanotube arrays. Bundling of nanotube creates additional pathway via intertube connection and decrease the internal surface area of the films accessible to dye molecules. Therefore, bundling of nanotubes increases the charge recombination and decreases the photoconversion efficiency. It was established that the high photocurrent density and photocurrent efficiency could be achieved by better-aligned nanotube arrays. Capillary stress creates the morphological disorder (e.g. bundling and microcracks) of TNTs during the solvent evaporation. Therefore, supercritical CO_2 drying process is developed for preparing crack-free and bundle-free nanotubes (Zhu et al., 2007). Many strategies have developed for the fabrication of TNTs such as direct electrochemical anodization of Ti foil,

electrophoresis, hydrothermal method, and incorporation of TiO_2 into anodized alumina oxide (AAO).

1-D nanostructures	Preparation method	Efficiency of 1-D nanostructures based DSSCs	Efficiency of NPs based DSSCs	Ref.
TiO_2 nanorod	Oriented attachment of nanoparticles	6.2%	4.2%	Kang et al., 2008
TiO_2 nanorod	Solvothermal	7.9%	5.5%	Marco et al., 2010
TiO_2 nanofibre/ TiO_2 nanoparticle	Electrospinning and sol-gel techniques	10.3%	9.25%	Chuangchote et al., 2008
Macroporous TiO_2 nanowires	Hydrothermal synthesis	0.86%	-	Wang et al., 2009
TiO_2 Nanotubes	Electrochemical anodization of Ti foils	3%	-	Zhu et al., 2007

Table 3. Comparison performance of different 1-D nanostructures photoelectrode with NPs based photoelectrode for the application in DSSCs

The other 1-D nanostrucutres are nanorods, nanowires, etc. Recently, Manca and coworkers have developed a novel and cost efficient method for the preparation of anatase TiO_2 nanorod (20-30 nm × 100-300 nm) by single-step solvothermal process (Marco et al., 2010). This single step solvothermal process does not require the complete removal of organic residual that will act as a binder. This TiO_2 nanorod showed improved photoconversion performance compared with the naocrystalline counterparts due to the increased rate of electron transport arisen from the high crystallinity of the nanorod. However, many reports suggested that the poor extent of dye loading and the poor light harvesting of nanorod based DSSC is due to the low specific surface area of the nanorod. To facilitate the improved dye loading, Kang et al. synthesized TiO_2 nanorod (4 nm × 20 nm) of high specific surface area from the necking of truncated NPs by "oriented attachment approach''(Kang et al., 2008). The improved roughness factor of the nanorod (169.9 μm^{-1}) compare to nanoparticles (115.6 μm^{-1}) showed higher dye absorption ability and thereby improved conversion efficiency. Intentional integration of metal impurities into the semiconducting materials is very useful and common approach for tuning the semiconducting properties such as band gap and electrical conductivity. Feng et al. prepared successfully tantalum (Ta)-doped TiO_2 nanowire by low temperature hydrothermal method. Ta-doped TiO_2 nanowire gives a very high photovoltage (0.87 V) of comparable J_{sc} with undoped naowire in a liquid-state DSSCs (Feng et al., 2009). The high open circuit potential close to the theoretical maximum might be attributed to the negative shift of flat band potential of nanowires. In table 3 we tabulate the comparison performance of DSSCs made by 1-D TiO_2 nanostructures and TiO_2 nanoparticles.

3.1.2 TiO_2 photoelectrode with scattering layer

The efficiency of DSSCs over 11% in laboratory scale has been reported (Grätzel, 2003). The ultimate target of DSSCs technology is the up scaling of the small cell into larger modules. Therefore, many important factors have to be considered such as stability, durability, and

more importantly price per watt of the module to bring the modules into market. Photosensitizing dye of high efficient DSSCs is still very expensive, so the actual cost-energy per watt of DSSCs module relies on the amount of dye usage. Many strategies such as development of organic dye, replacement of platinum by carbon materials and organic polymer have been developed for the reduction of energy cost of DSSCs. However, one remarkable strategy has been developed on the modification of TiO_2 photoelectrode is the uses of scattering (SC) TiO_2 particles (films or mixed with nanocrystalline particles). These SC layer/particles will help to develop very thin nanocrystalline TiO_2 film of high surface area that will reduce the dye usage without sacrificing the cell efficiency. Figure 8 shows the light confined effect on different TiO_2 particles. It can be seen that SC TiO_2 particles scattered the incident longer wavelength light and prolonged the optical path length. Hence, the transmitted visible light can effectively uses for photon conversion. However, light scattering property is strongly dependent on the refractive index between the active TiO_2 film, scattering layer, and on the relative size of the scattering particles (Shin et al., 2010; Arakawa et al., 2006).

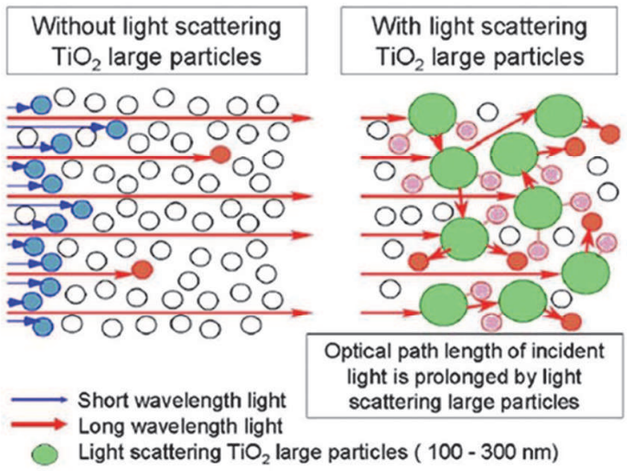


Fig. 8. Conceptual scheme of Light confined effect (reproduced with permission from ref. Arakawa et al., 2006. Copyright 2010, IEEE)

Scattering layer (SC) matrix	V_{oc} (mV) with SC (without SC) layer	J_{sc} (mAcm^{-2}) with SC (without SC) layer	FF (%) with SC (without SC) layer	η (%) with SC (without SC) layer	Ref.
TiO_2 film of 300 nm particles	735 (680)	14.5 (12.3)	No appreciable change	7.48 (5.77)	Kim et al., 2008
sub-micrometer-sized Al_2O_3	745 (730)	14.44 (12.54)	71.1 (67.7)	7.3 (6.5)	Shin et al., 2010
ZrO_2(500-1000 nm)	738 (710)	12.72 (6.42)	61.8 (70.2)	5.8 (3.2)	Hore et al., 2006
ZnO microsheets	677 (636)	8.68 (6.04)	43.98 (46.58)	2.58 (1.79)	Yi et al., 2010

Table 4. Summarization of the performance of different scattering particles based photoelectrode for the application in DSSCs

Hore et al. investigated the comparison study of the performance of different thickness (4 µm, 8 µm) of nanocrystalline TiO_2 film of high surface area with and without scattering layer (Hore et al., 2006). It was observed that the 4 µm nanocrystalline TiO_2 thin film with SC layer shows a comparable performance with 8 µm thick TiO_2 film without SC layer. Therefore, it is expected to use thin film of TiO_2 with SC layer for the industrial production of large DSSC modules, which will minimize the cost of dye by lesser consumption in the production procession. Some other metal oxide has also explored as effective SC layer on top of the active TiO_2 film such as ZrO_2, Al_2O_3, TiO_2-rutile form, ZnO etc. Table 4 summarizes the comparison of photoconversion efficiencies with different scattering particles.

3.1.3 Metal-doped titania (TiO_2) photoelectrode

Metal-ions as dopant has a significant effect on the electrical surface state modification of TiO_2. This modification leads to significant change of electrical conductivity, shifting of Fermi level potential, particle aggregation, charge transfer kinetics, and dye absorption characteristics of TiO_2. However, many reports have suggested that the performance of DSSCs at the optimized level of metal-ions doping into TiO_2 differ mainly the tuning of flat band of TiO_2. Lü et al. synthesized well-crystalline niobium (Nb) doped anatase TiO_2 (Nb-TiO_2) and investigated its effect on the performance of DSSCs (Lü et al., 2010). It was revealed that Nb doping level of 2.5 -7.5 mol% has positive effect on the short circuit current with positive shift of flat band potential. This increment of the photocurrent was attributed to the enhanced electron injection, increased charge transfer kinetics as well as the improvement of dye loading up to $5.7\pm0.2x10^{-8}$ [mol cm^{-2}] at a doping level of 7.5 mol% compared to the undoped state. The TiO_2 doped by various metals such as tungsten (W), neodymium (Nd) also exhibited the similar phenomenon (Ko et al., 2005; Yao et al., 2006), while Al doped TiO_2 showed an opposite effect (Ko et al., 2005). Lee et al. deposited a thin film of compact Nb-doped TiO_2 on FTO by pulsed laser deposition (PLD) (Lee at al., 2009). The performance of the DSSC of compact Nb-doped TiO_2 layer with an upper mesoporous TiO_2 layer is prominent compared to the compact TiO_2 layer.

Figure 9 describes the band diagram of two compact layers and the charge transfer kinetics. The upper part of the diagram is before contact with FTO and it can be seen that the Fermi level of compact TiO_2 and Nb-doped TiO_2 layers is below and above of the conduction band (E_{CB}) respectively. This is ascribed by the degeneracy of Nb-doped TiO_2 and the nondegeneracy of compact TiO_2. When compact TiO_2 and FTO are in contact (i.e. semiconductor–metal contact), a depletion region or Schottky barrier, q (φ_m-φ_s) is form by the difference of work function of FTO (φ_m) and TiO_2 (φ_s). Electrons have to overcome this barrier in order to be transferred from compact TiO_2 to FTO. Hence, the electron injection efficiency is decreased while the back electron transfer was increased. On the other hand, the contact between FTO and the compact degenerate Nb-doped TiO_2 layer form a very narrow depletion region. Electrons injected rapidly from compact Nb-doped TiO_2 to FTO by tunneling leads to ohmic contact characteristics (Lee et al., 2009). Therefore, the incorporation of compact Nb-doped TiO_2 layer remarkably reduces the interfacial charge transfer resistance and results in the enhancement of the performance of the DSSC. The performance of some of the metal-doped TiO_2 nanocompisites in DSSCs is summarized in table 5. From the experimental data of table 5, it is clearly observed that doped metal ions have a strong effect for the tuning of flat band potential, as well as the electron injection efficiency.

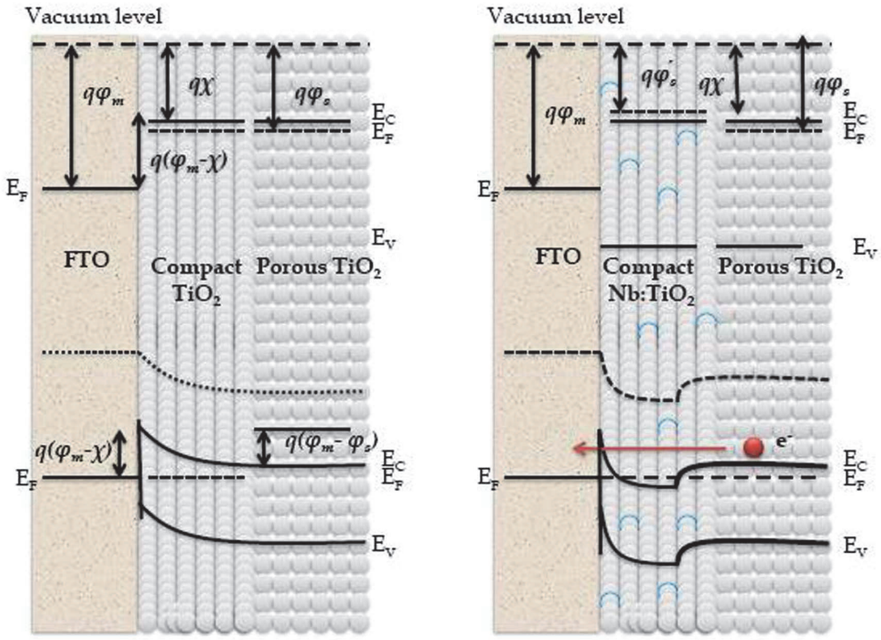


Fig. 9. Schematic illustration of band diagram of compact TiO_2 and compact Nb-TiO_2 layer before (upper) and after (under) contact with FTO (redrawn with permission from, Lee at al., 2009. Copyright 2010, The American Chemical Society)

Dopant	Synthesis techniques	V_{oc} (mV) of doped (undoped) TiO_2	J_{sc} ($mAcm^{-2}$) of doped (undoped)	FF (%) of doped (undoped)	η (%) of doped (undoped)	Ref.
5mol% Nb	Hydrothermal synthesis	700 (790)	17.67 (11.87)	63 (70)	7.8 (6.6)	Lü et al., 2010
Nd	Solvothermal reactions	701 (707)	13.1 (10.7)	40.1 (36.6)	4.4 (3.3)	Yao et al., 2006
Bi	Sol–gel	590 (570)	7.71 (5.52)	46 (38)	2.11 (1.19)	An'amt et al., 2010
Ta	Hydrothermal	870 (~750)	7.5 (8.1)	63 (68)	4.1 (4.06)	Feng et al., 2009

Table 5. Summarization of the performance of different metal-doped TiO_2 and undoped TiO_2 photoelectrodes for the application in DSSC

3.1.4 Core-shell composite of titania (TiO_2) and other metal-oxide for photoelectrode

Coating of TiO_2 with different metal oxide/hydroxide of wide band gap such as MgO, Nb_2O_5, ZnO, $SrTiO_3$, $Mg(OH)_2$, $Zn(OH)_2$ etc has received much attention for the improvement of the performance of DSSCs. Metal oxide/hydroxide coating on TiO_2 employed a core-shell structure, which is advantageous for the efficient photoconversion. Firstly, the wide band gap of shell metal oxide minimizes the electron-hole recombination by increasing the surface resistance of TiO_2 and retards the back electron transfer to the electrolyte. Secondly, the shell layer increases the dye absorption due to increased surface

area leading to high photoconversion and finally tuning the conduction band of core structure (Jung et al., 2005). Figure 10 depicts the different core-shell structure of metal oxide. The use of a thin metal oxide/hydroxide layer (shell) permitted the formation of an energy barrier at the electrode/electrolyte interface. It reduced the recombination rate and thereby improved the cell performance. The core-shell structure C in Figure 10 is favorable for the diffusion of the injected electrons because it does not face any energy barriers during the electron diffusion to the FTO (Chappel et al., 2002).

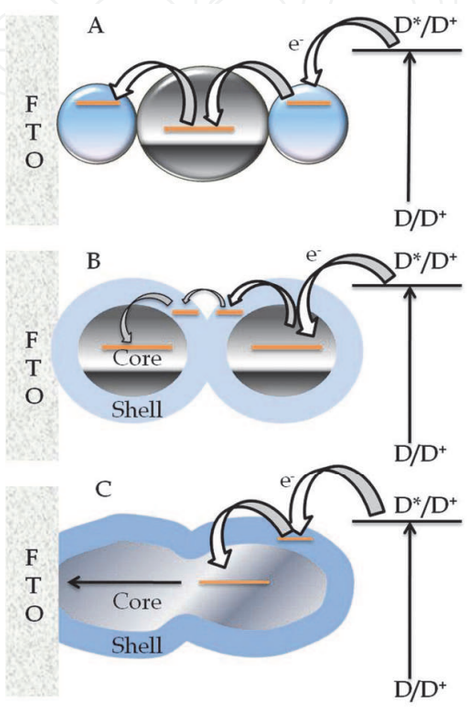


Fig. 10. Different geometries of core-shell electrodes showing that only in the core-shell matrix (c) the photoinjected electrons does not face any energy barriers during the diffusion to the TCO (redrawn with permission from, Chappel at al., 2002. Copyright 2010, The American Chemical Society)

Chen et al. prepared a new bilayer of Nb_2O_5 coated nanoporous TiO_2 photoelectrode (Chen et al., 2001). The conduction band of shell materials Nb_2O_5 is 100 mV negative than the core materials TiO_2. Thus, the Nb_2O_5 form an energy barrier to the photoelectrode and, therefore, confined the electrons to the core TiO_2 particles. This electron confinement to TiO_2 particles reduces the recombination and thereby increases the J_{sc}. The increase of the photovoltage is attributed to the shift of the Fermi level of TiO_2 towards negative direction by Nb_2O_5 (schematically describe in figure 11A). Consequently, all the cell parameter was improved and the overall cell efficiency enhanced up to 35%. Diamant et al. reported the development of $SrTiO_3$ coated TiO_2 photoelctrode. The conduction band of $SrTiO_3$ is 200 mV negative than that of TiO_2 (Diamant et al., 2003). This suitable band position of core-shell composite resulted in the increment of J_{sc} by the reduced recombination as well as the efficient electron injection to FTO. Increment of V_{oc} is attributed to the pervious phenomenon as Nb_2O_5-TiO_2 core shell photoelectrode. As a result, the overall DSSCs performance increased by 15%.

Nonmetal oxides such as $CaCO_3$ with high band energy (6.0 eV) for the formation of favorable core-shell with TiO_2 and high isoelectric point (IEP) to improve dye loading have also been explored. The increment of J_{sc} is mainly due to the high specific surface area of the $CaCO_3$ overlayer that caused the enhancement of dye loading up to 54%. The increased photovoltage is also attributed to the phenomenon described above with the more negative conduction band edge of $CaCO_3$ compare to that of TiO_2. Overall, photo conversion increased by 24.4% with this approach (Lee at al., 2007).

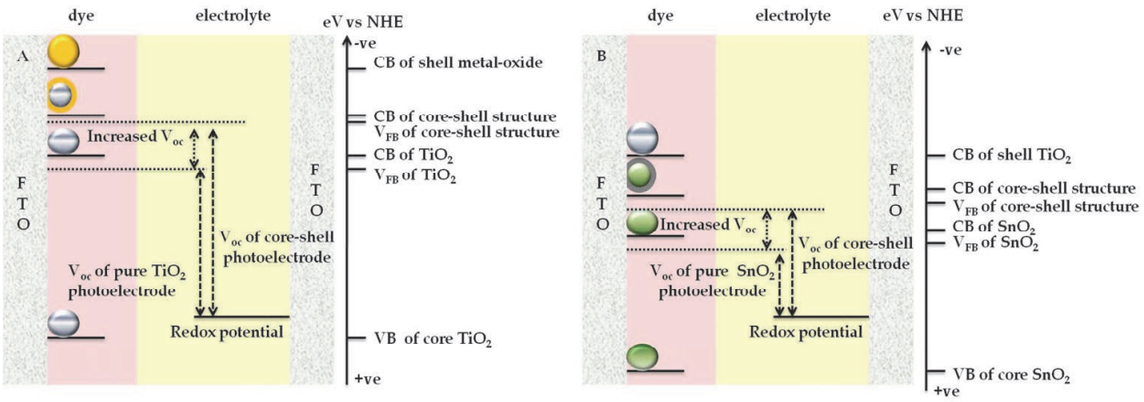


Fig. 11. Schematic illustration of energy band tuning of TiO_2 photoelectrode (A) and SnO_2 photoelectrode (B) by the introduction of core-shell structure

The lower conduction band edge of SnO_2 compare to rutile TiO_2 makes it possible to switch the core-shell structure (i.e. TiO_2 as shell matrix and SnO_2 as core matrix). Reports are available for the formation of rutile TiO_2 coated SnO_2 hollow microsphere and nanoparticles. Qian et al. fabricated rutile TiO_2 coated SnO_2 hollow microsphere (MHS) for DSSCs photoelectrode (Qian et al., 2009). The Core-shell structure was characterized by scanning electron microscope (SEM), high-resolution transmission-electron microscope (HR-TEM), and x-ray diffraction (XRD). The XRD pattern of TiO_2-MHS is well indexed with the rutile structure of SnO_2 [space group *P42/mnm* (136)] with the additional rutile TiO_2 characteristics peak observed at 2θ = 36.09, 41.22, and 54.32^0. The open circuit potential of TiO_2-SnO_2 MHS photoelectrode (V_{oc} = 0.664 V) was higher than that of the pure SnO_2 photoelectrode (V_{oc} = 0.398 V) but lower than that of pure anatase TiO_2 photoelectrode (V_{oc} = 0.697 V). This is attributed to the fact that the conduction band of SnO_2 is 300mV more positive than the rutile TiO_2. Upon TiO_2 modification by SnO_2 MHS, the electronic band shifts to a more negative value (schematically describe in figure 11B). The open-circuit potential of TiO_2–SnO_2 MHS is improved greatly. This indicates the effective suppression of interfacial electron recombination in TiO_2–SnO_2 MHS electrode. J_{sc} of the core-shell photoelectrode was observed higher than that of pure anatase TiO_2 photoelectrode. This is responsible for the formation of favorable energy barrier for efficient electron injection as depicted in figure 10C as well as the concurrent decrease of the recombination with increasing the surface resistance of SnO_2. Chappel et al. observed a similar phenomenon by using rutile TiO_2 coated SnO_2 nanoparticle (Chappel et al., 2002). The different core-shell nanostructures photoelectrode and their performance for the application in DSSCs are summarized in Table 6.

Core-shell	Synthesis techniques	V_{oc} (mV) of modified (unmodified)	J_{sc} (mAcm^{-2}) of modified (unmodified)	FF (%) of modified (unmodified)	η (%) of modified (unmodified)	Ref.
MgO-Coated TiO_2 NPs	Topotactic reaction	720 (640)	11.7 (10.2)	53.5 (47.3)	4.5 (3.1)	Jung et al., 2005
Nb_2O_5 Coated TiO_2	Hydrothermal	730 (661)	11.4 (10.2)	51 (56.5)	4.97 (3.62)	Wang et at., 2001)
$SrTiO_3$ coated TiO_2	Hydrothermal	708 (650)	10.2 (10.5)	58.4 (53.6)	4.39 (3.81)	Diamant et al., 2003
$CaCO_3$-Coated TiO_2	Topotactic thermal decomposition	668 (654)	21.92 (19.39)	66.1 (61.8)	9.68 (7.84)	Lee et al., 2007
$Mg(OH)_2$ coated TiO_2	Cathodic deposition	758 (696)	6.61 (6.43)	74 (73.6)	3.7 (3.3)	Yum et al., 2006
TiO_2 coated SnO_2 MHS	Sol-gel	664 (697)	14.6 (11.07)	58.3 (66.6)	5.65 (5.14)	Qian et al., 2009

Table 6. Comparison performance of different core-shell modified and unmodified TiO_2 and SnO_2 photoelectrode for the application in DSSCs

3.2 Photoelectrode based on ZnO and its composite

Zinc oxide (ZnO) is an important class of semiconductor. It is almost insoluble in water, usually appears as white powder, and exists in nature usually as zincite mineral. Many superior physical properties such as the high electron mobility (~100 cm^2/Vs), high thermal conductivity and stability, wide and direct band gap (E_g = ~3.37 eV at room temperature), large excitation binding energy (60 meV), large saturation velocity (3.2x10^7 cms^{-1}) and high optical gain of 300 cm^{-1} (100 cm^{-1} for GaN) at room temperature make it as an attractive materials for wide range of application such as sensor, pigments in paint, filler in rubber products, thin film transistor, photodetectors, light emitting diode(LED) and in photovoltaic device (Rahman et al.,2010). The electronic configuration of ZnO is composed by completely filled 3*d*-orbital ($3d^{10}$). The valence band of ZnO consists of only *d* orbital and the conduction band is composed by hybridized *s–p* orbitals. This type of electronic configuration of ZnO leads to the state of dissimilar parity with reduced (e^--h^+) recombination probability (Jose et al., 2009). Therefore, from the point of view of electronic configuration and excellencies in physical properties, ZnO is considered as a suitable material for the application in DSSC. There are three crystalline forms for ZnO: hexagonal wurtzite, cubic zincblende, and cubic rock salt. Among them, wurtzite is the most stable at ambient condition, lowest energy

structure, and most common form of crystal. Cubic zincblende can also be stabilized by growing cubic ZnO on substrate. However, the cubic rock salt (NaCl) type ZnO is observed very rarely at extremely high pressure of 10 G pa (Corso et al., 1994). Figure 12 shows the structure of two crystallographic form of ZnO (wurtzite and cubic zincblende), where the zinc (Zn) and oxygen centers are tetrahedral. The conduction band energy of hexagonal wurtzite ZnO is similar to that of the conduction band of TiO_2. That's why; the hexagonal wurtzite ZnO has extensively explored for the development of efficient DSSCs and for the replacement of TiO_2 as well (Redmond et al., 1994). In this section, we will discuss on the potential application, prospects, and limitation of ZnO based photoelectode for the application in DSSCs.

Hupp and colleagues studied the electron transport properties in ZnO nanotube (64μm length) by EIS. It was observed that the electron transport is significantly faster and electron extracted more rapidly in ZnO nanotube compare to nanocrystalline TiO_2 (Martinson et at., 2009). On the other hand, Hagfeldt and coworkers suggested that the electron diffusion follows a trapping/detrapping mechanism in nanoporous ZnO. This trapping/detrapping is strongly dependent on the variation of film thickness, applied potential, and electrolyte system (Solbrand et al., 2000). It is estimated that the diffusion coefficient in ZnO photoelectrode is 10^{-6} cm^2s^{-1} at +300 mV vs Ag/AgCl in ethanol with 0.5 M $LiClO_4$ and $2x10^{-5}$ cm^2s^{-1} for nanoporous TiO_2 electrode under the same condition but in 0.7 M $LiClO_4$. Therefore, electrons are more long lived in ZnO than in TiO_2 and that the electron losses to acceptors in solution and to deep traps are less for ZnO than for TiO_2. Despite these superior physical properties of ZnO, the highest reported efficiency of ZnO based DSSCs is still very low (*ca.* 6.58%). This might be due to the formation of Zn^{2+}/dye complex that inhibits the efficient electron injection and causes the retardation of the dye regeneration. The highly efficient acidic ruthenium (II) dyes (such as N3, N719, Black dye, etc.) generally showed lower performance with ZnO based photoelectrodes. It was attributed to the reduced chemical stability of ZnO due to the dissolution of ZnO and formation of aggregates which are caused by the proton release from the acidic dye. In order to improve the performance and stability of ZnO based photoelectrode, different strategies have been introduced. It includes the design and synthesis of suitable new dyes for ZnO photoelectrode, the development of quantum dot (QD) sensitized ZnO photoelectrode, and the development of 1-D ZnO photoelectrode for efficient photoelectron collection (Quintana et al., 2007; Zhang et al., 2009).

As discussed in the figure 7D, 1-D nanostructure makes the unidirectional electron diffusion possible and therefore increases the efficiency of electron injection and collection by reducing the recombination during the interparticle hopping process. Various types of 1-D ZnO, such as hierarchical ZnO nanowire-nanosheet, nanodisk, nanowire, nanorod, nanofibre, and nanocomb have been synthesized for the application in DSSCs. Figure 13 depicts the scanning electron microscopic (SEM) images of some of the 1-D ZnO nanostructures. Umar et al. fabricated highly crystalline ZnO nanocomb directly grown on FTO by noncatalytic hydrothermal evaporation process (Umar et al., 2009). However, ZnO nanocomb photoelectrode with N719 sensitization showed very low conversion efficiency of 0.86%, due to the low dye loading and fast interfacial recombination of electron and holes. The former is attributed to the low specific surface area of 1-D nanostructures of ZnO. This concurrently results in the increases of the recombination due to the enhancement of charge recombination at the uncovered oxide surface. This effect was minimized by the development of 1-D nanostructure with high aspect ratios and the various 1-D

nanostructures of ZnO used for DSSCs are summarized in Table 7. In brief, Wang et al. synthesized porous hierarchical ZnO nanodisk with higher surface area (21.8 m^2g^{-1}) by a simple low temperature hydrothermal method (Wang et al., 2010). Ramakrishna et al. developed ZnO nanofibres with even higher aspect ratio and surface area of 30 m^2g^{-1} (Zhang et al., 2009). Both showed the improvement of efficiencies up to 2.49 and 3.02% respectively mainly due to the improved dye loading.

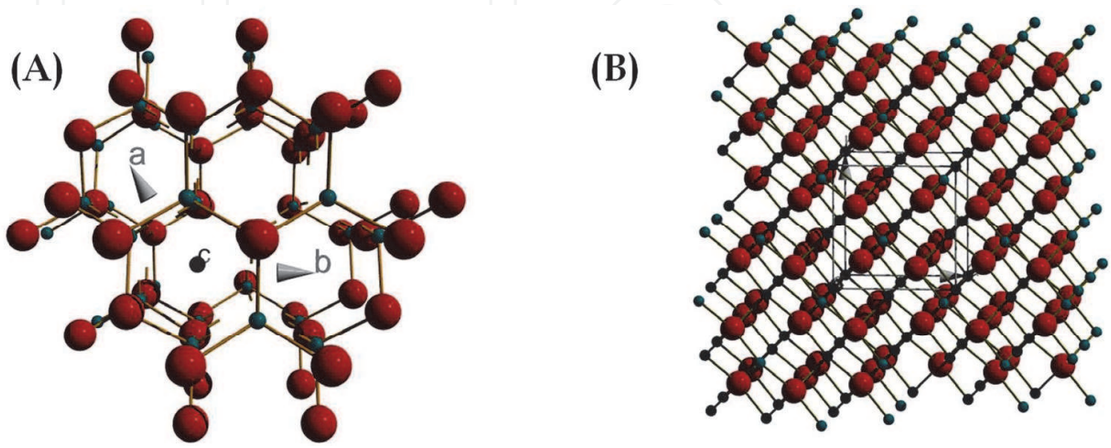


Fig. 12. Crystallographic pattern of mostly observed and common hexagonal wurtzite crystal of ZnO (space group *P 63mc*) (a) and cubic zincblende (space group *F 43m*) (b). Where big red sphere Zn^{2+}, small green sphere: O^{2-}

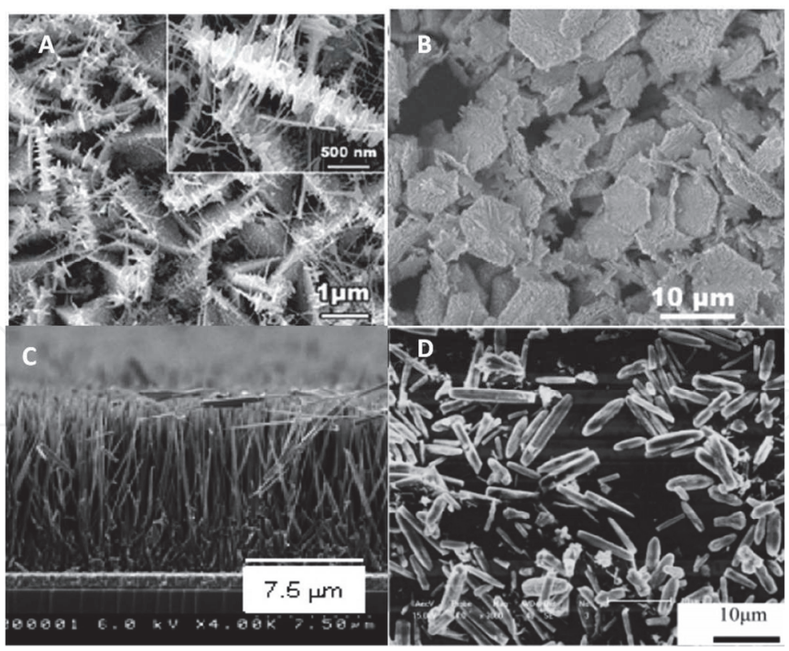


Fig. 13. Scanning electron microscopic (SEM) image of different 1-D nanostructures of ZnO (A) Hierarchical ZnO nanowire-nanosheet,(B) nanodisk,(C) nanowire, and (D) nanorod.(reproduced with permission for ref. Xu et al., 2010; Wang et al., 2010; Gao et al., 2007; Pang et al., 2007. Copyright 2010, The American Chemical Society)

Materials	Synthesis process	Surface area (m^2g^{-1})/ aspect ratio	Sensitizer	V_{oc} (V)	J_{sc} ($mAcm^{-2}$)	FF (%)	η (%)	Ref.
ZnO nanocomb	Noncatalytic Thermal evaporation	-	N719	0.67	3.14	34	0.68	Umar et al., 2009
ZnO nanowire	Hydrothermal	-/100-120	N719	0.54	6.79	50	1.7	Gao et al., 2007
ZnO nanorod	Hydrothermal	12.71/-	N719	0.73	3.41	74.4	1.86	Umar et al., 2009
ZnO nanodisk	Hydrothermal	21.8/-	N719	0.69	6.92	52.5	2.49	Wang et al., 2010
ZnO nanofibre	Electrospinning	30/-	N719	0.57	9.14	58	3.02	Zhang et al., 2009

Table 7. Summarization of different 1-D ZnO nanostructures, their physical properties, along with their performance in DSSCs

ZnO has been extensively explored as a composite material together with TiO_2 for the application in DSSCs. The potential application of ZnO nanostructures as a scattering layer and core-shell nanostructures composites along with TiO_2 has described in section 3.1.2 and 3.1.4. In this section, we need more focus on the hybrid nanocomposites of ZnO for the application in DSSC. In addition to the development of 1-D ZnO nanostructures with higher aspect ratio and surface area, many ZnO nanocomposites (shown in figure 14) have explored to improve the dye loading with maintaining the directional electron transport pathway as in 1-D nanostructures.

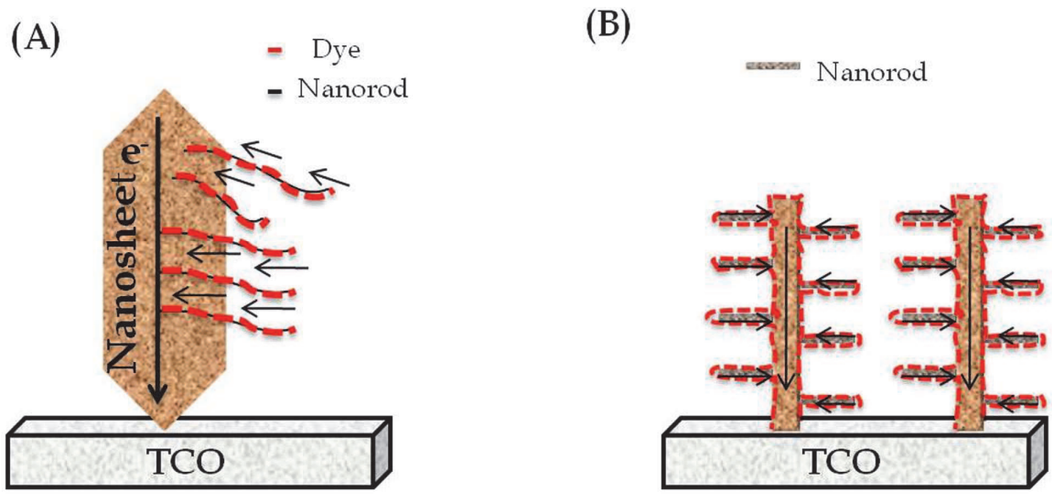


Fig. 14. Schematic illustration of different types of nanocomposites, (A) Hierarchical ZnO nanowire-nanosheet, (B) branched ZnO nanorod along with their directional electron transport. (redrawn with permission from ref. Xu et al., 2010; Cheng at al., 2008. Copyright 2010, The American Chemical Society)

Cheng et al. fabricated a branched ZnO nanowire on FTO by hydrothermal method. The fabricated branched nanowires consists perpendicular and outspread branched nanowires (Cheng et al., 2008). The phototconversion efficiency of the branched nanowires is almost twice than that of ZnO nanowire. The enhancement of photocurrent was attributed to the increase of internal surface area of the branched structure for higher dye loading without the increase of interparticle hopes. The extended nanocomposites with extended optical path length were also partly responsible for higher photoconversion efficiency due to more light scattering. Jiang et al. introduced a flower like branched ZnO nanowires, that yields higher photconversion efficiency compare to the upstanding ZnO nanowire array (Jiang et al., 2007). Subsequently, Xu et al. synthesized hierarchical ZnO nanoarchitectures, consisting of ZnO nanosheet array on indium tin oxide (ITO) glass followed by the chemical growth of ZnO nanowires on the nanosheets array (Xu et al., 2010). The photoconversion efficiency (*ca*. 4.8%) of this nanoarchitecture is more than double compare to its nanosheet counterpart photoelectrode. Table 8 shows the phoconversion parameters of some reported nanocomposites used for DSSCs.

Nanocomposites	Sensitizer	V_{oc} (mV)	J_{sc} (mAcm$^{-2)}$	FF (%)	η (%)	Ref.
ZnO nanowire array/nanoparticle	Mercurochrome	610	6.3	580	2.2	Ku & Wu, 2007
ZnO nanoflower	N719	650	5.5	53	1.9	Jiang et al., 2007
Branched ZnO Nanowires	N719	675	4.27	52.2	1.51	Cheng et al., 2008
ZnO Nanowire-Nanosheet	N719	680	10.9	65	4.8	Xu et al., 2010

Table 8. Comparison of the photoconversion performance of different ZnO nanocomposite based photoelectrode in DSSCs

3.3 Photoelectrode based on Nb_2O_5 and $SrTiO_3$

Niobium pentaoxide (Nb_2O_5) is another important type of wide band gap (E_g= ~3.49 eV) semiconductor and has been investigated for the development of photoelectrode materials for DSSCs. Nb_2O_5 is appreciably explored as composite materials with TiO_2 as a core-shell structure discussed it the section 3.1.4. The higher band position of Nb_2O_5 up to 250 mV relative to the TiO_2 makes it suitable for the formation of core-shell structure (Wei et al., 2008). Nb_2O_5 has two different crystal structures of monoclinic and orthorhombic with the space group *P2* and *Pbam,* respectively. The cell parameters of monoclinic crystal are a = 2038, b = 3.824, and c = 19.37 Å with β = 115.69^0 and for orthorhombic crystal, a = 6.168, b = 29.31, and c= 3.935 Å (Jose et al., 2009). The large unit cell dimension of Nb_2O_5 is partly responsible for the reduction of surface area. The reduced surface area of Nb_2O_5 causes the inefficient dye loading and results in the decrease of short circuit current. GuO et al. developed a single-crystal Nb_2O_5 photoelectrode for the fabrication of DSSCs (Guo et al., 1999). The low surface area of the Nb_2O_5 (25 m^2g^{-1}) compare to TiO_2 (104 m^2g^{-1}) showed relatively poor performance in DSSCs. Random movement of the injected electron into the single-crystal Nb_2O_5 might be another factor for decreased photocurrent. Therefore, the efficiency of the DSSCs (active area 0.2 cm^2) decreases from 5.0 to 2.2%. For scaling up the

performance of Nb_2O_5 based DSSCs, Wei et al. synthesized 1-D Nb_2O_5 nanobelts for directional transport of electron to increase the photocurrent (Wei et al., 2008). Nevertheless, the main drawbacks of 1-D nanostructures are the drop off of surface area with decreased aspect ratios. Therefore, the decrease dye loading of the nanobelts results the poor conversion efficiency. It is noteworthy that the higher stability, higher conduction band energy of Nb_2O_5 could be makes it suitable materials for the development of high efficient DSSCs like TiO_2. Therefore, researchers should give more attention to develop the nanoporous Nb_2O_5 nanoparticles and well defined 1-D nanostructures with different nanocomposites for the fabrication of DSSCs.

$SrTiO_3$ is a binary metal-oxide with high dielectric constant (~10^4) and shares more structural similarities with anatse TiO_2. Figure 15 depicts the perovskite-type cubic structure of $SrTiO_3$ of space group *Pm3m* and lattice parameter a = 3.9. Titanium atoms are in 6-fold octahedral coordination in $SrTiO_3$, similar to the titanium arrangement in anatase TiO_2 (Lotnyk et al., 2007). The band gap of $SrTiO_3$ is ~3.2 eV and the conduction band is 0.2 eV above the conduction band of anatase TiO_2. This suitable band position of $SrTiO_3$ makes it appropriate materials for the development of DSSCs photelectrode (Burnside et al., 1999). We described the core-shell structure of TiO_2-$SrTiO_3$ in the section 3.1.4. In spite of the similar band gap of $SrTiO_3$ and anatase TiO_2, the negative positioned of the conduction band of $SrTiO_3$ leads to the negative shift of the flat band (V_{FB}) of $SrTiO_3$. Therefore, the application of pure $SrTiO_3$ as photoelectrode will increase the photovoltage of DSSC.

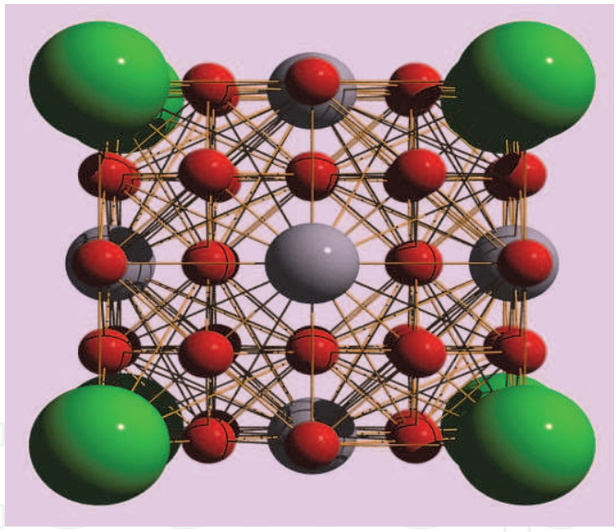


Fig. 15. Crystallographic pattern of perovskite-type cubic structure of $SrTiO_3$ (space group Pm3m), where, big green sphere: Sr^{2+}, grey sphere: Ti^{4+}, and small red sphere: O^{2-}.

Burnside et al. synthesized nanocrystalline $SrTiO_3$ by hydrothermal treatment for the application in DSSCs (Burnside et al., 1999). The prepared photoelctrode sensitized by ruthenium (2, 2′-bipyridyl-4, 4′-dicarboxylate)$_2$(NCS)$_2$) showed the expected increment of V_{oc} (789 mV) compare to TiO_2 (686 mv). However, the photoconversion efficiency is very low due to the decreased J_{sc}. This might be due to the decreased surface area of nanocrystalline $SrTiO_3$, lack of directional movement of electrons and the low dye uptake. In order to increase the performance of $SrTiO_3$ based DSSCs, research should be focused to develop new techniques for synthesizing highly porous nanoparticles of reduced size, 1-D

nanostructures for the efficient injection of electrons and to retard the recombination. Development of new dyes with more negative positioned LUMO level compare to other conventional dye would be another interest of research of $SrTiO_3$ based DSSC. In this respect, Zaban and coworkers, developed a type-II DSSCs by utilizing $SrTiO_3$ coated TiO_2 for efficient electron injection by minimizing the back reaction (Hod et al., 2010). Since the conduction band of $SrTiO_3$ is more negative than TiO_2 and the LUMO of type-II sensitizer (catechol) is well above the conduction of TiO_2. Therefore, coating of TiO_2 with $SrTiO_3$ creates an energy barrier for efficient electron transfer from $SrTiO_3$ to TiO_2 and reduces the back electron transfer from oxidized dye. So an increase of J_{sc} (18%) and 70% charge collection improved the performance of DSSCs. No reports are available for the development of 1-D nanostructures of $SrTiO_3$ and its application in DSSC. Therefore, more attention should be required for the development of 1-D nanostructure of $SrTiO_3$ with high aspect ratios and exploring different dye for type-I and for type-II DSSCs.

4. Conclusion

This chapter discussed the structural aspects of various metal oxides and their composites. Interfacial electron transfer kinetics of dye/metal oxides and metal oxide/electrolyte for the conventional DSSCs were discussed. The alteration of interfacial electron transfer kinetics upon modification of the photoelectrode with metal oxide composite has also been described. In addition to the performance of different metal oxides and their composites in DSSC photoelectode, the fundamental aspects, the characterization methods, and the prospects and limitations of DSSCs were briefly explained. Various strategies for the sequential development of highly efficient DSSCs have been described and suggested nevertheless not satisfactory yet for the commercialization of DSSCs with high efficiency. The authors wish that this chapter can guide the researchers to understand the fundamental aspect and the stepwise development of different metal oxides and their composite for the photoelectrode of DSSCs.

5. Acknowledgement

This work was supported by the National Research Foundation of Korea (NRF) grant funded by the Korea government (MEST) (No. 2008-0062166) and Korea Research Foundation Grant funded by the Korean Government (MOEHRD, Basic Research Promotion Fund) (KRF-2007-211-C00029). It was also supported partly by Seoul R&BD Program (WR090671) and by the New & Renewable Energy program of the Korea Institute of Energy Technology Evaluation and Planning (KETEP) grant funded by the Korea government Ministry of Knowledge Economy.

6. References

Arakawa, H.; Yamaguchi, T.; Takeuchim, A. &Agatsuma, S. (2006). Efficiency improvement of dye-sensitized solar cell by light confined effect, *Conference Record of the 2006 IEEE 4th World Conference on Photovoltaic Energy Conversion*, pp. 36-39, 1-4244-0017-1, Waikoloa, HI,May2006, IEEE, New York.

An'amt, M.N.; Radiman, S.; Huang, N.M.; Yarmo, M.A.; Ariyanto, N.P.; Lim, H.N. & Muhamad, M.R. (2010). Sol–gel hydrothermal synthesis of bismuth–TiO_2

nanocubes for dye-sensitized solar cell. *Ceram. Int.*, 36, 7, (September2010), 2215–2220, doi:10.1016/j.ceramint.2010.05.027.

Burnside, S.; Moser, J.-E.; Brooks, K. & Grätzel, M. (1999). Nanocrystalline Mesoporous Strontium Titanate as Photoelectrode Material for Photosensitized Solar Devices: Increasing Photovoltage through Flatband Potential Engineering. *J. Phys. Chem. B,* 103, 43, (August 1999), 9328-9332, DOI: 10.1021/jp9913867.

Benkstein, K. D.; Kopidakis, N.; Van de Lagemaat, J. & Frank, A. J. (2003). Influence of the Percolation Network Geometry on Electron Transport in Dye-Sensitized Titanium Dioxide Solar Cells. *J. Phys. Chem. B*, 107, 31, (July2003) 7759–7767, DOI: 10.1021/jp022681l.

Bisquert, J.; Cahen, D.; Hodes, G.; Rühle, S. & Zaban, A. (2004). Physical Chemical Principles of Photovoltaic Conversion with Nanoparticulate, Mesoporous Dye-Sensitized Solar Cells. *J. Phys. Chem. B,* 108, 24, (May 2004), 8106-8118, DOI: 10.1021/jp0359283.

Bergeron, B. V.; Marton, A.; Oskam, G. & Meyer, G. J. (2005). Dye-Sensitized SnO_2 Electrodes with Iodide and Pseudohalide Redox Mediators. *J. Phys. Chem. B,* 109, 2, (December 2005), 937-943, DOI: 10.1021/jp0461347.

Corso, D. A.; Posternak, M.; Resta, R. & Baldereschi, A. (1994). Ab initio study of piezoelectricity and spontaneous polarization in ZnO. Phys. Rev. B, 50, 15, (June 1954), 10715-10721, DOI:10.1103/PhysRevB.50.10715.

Chen, S.G.; Chappel, S.; Diamant, Y. & Zaban, A. (2001). Preparation of Nb_2O_5 Coated TiO_2 Nanoporous Electrodes and Their Application in Dye-Sensitized Solar Cells. *Chem. Mater.*, 13, 12, (November 2001), 4629-4634, DOI: 10.1021/cm010343b.

Chappel, S.; Chen, S.-G. & Zaban, A. (2002). TiO_2-Coated Nanoporous SnO_2 Electrodes for Dye-Sensitized Solar Cells. *Langmuir*, 18, 8, (March 2002), 3336-3342, DOI: 10.1021/la015536s.

Cheng, H.-M.; Chiu, W.-H.; Lee, C.-H.; Tsai, S.-Y.& Hsieh, W.-F. (2008). Formation of Branched ZnO Nanowires from Solvothermal Method and Dye-Sensitized Solar Cells Applications. *J. Phys. Chem. C,* 112, 42, (September 2008), 16359–16364, DOI: 10.1021/jp805239k.

Chuangchote, S.; Sagawa, T. & Yoshikawa, S. (2008). Efficient dye-sensitized solar cells using electrospun TiO_2 nanofibers as a light harvesting layer. *Appl. Phys. Lett.*, 93, 3, (July2008), 033310, 0003-6951.

Diamant, Y.; Chen, S. G.; Melamed, O. & Zaban, A. (2003). Core-Shell Nanoporous Electrode for Dye Sensitized Solar Cells: the Effect of the $SrTiO_3$ Shell on the Electronic Properties of the TiO_2 Core. *J. Phys. Chem. B*, 107, 9, (February2003), 1977-1981, DOI: 10.1021/jp027827v.

EIA panel report on International energy outlook 2010 (IEO2010), July 2010, DOE/EIA-0484(2010), US department of Energy, Washington, DC 20585.

Fujishima, A. & Honda, K. (1972). Electrochemical photolysis of water at a semiconductor electrode. *Nature*, 238, (July1972), 37–38, doi: 10.1038/238037a0.

Fabregat-Santiago,F.; Bisquert,J.; Palomares,E.;Otero,L.; Kuang,D.; Zakeeruddin,S.M.; Gra1tzel,M.(2007). Correlation between Photovoltaic Performance and Impedance Spectroscopy of Dye-Sensitized Solar Cells Based on Ionic Liquids. *J. Phys. Chem.*, 111, 17, (April 2007), 6550-6560, DOI: 10.1021/jp066178a.

Feng, X.; Shankar, K.; Paulose, M. & Grimes, C. A. (2009). Tantalum-Doped Titanium Dioxide Nanowire Arrays for Dye-Sensitized Solar Cells with High Open-Circuit Voltage. *Angew. Chem. Int. Ed.*, 48, 43, 8095 –8098, DOI: 10.1002/anie.200903114.

Guo, P. & Aegerter, M. A. (1999). Ru(II) sensitized Nb_2O_5 solar cell made by the sol-gel process. *Thin Solid Films*, 351, (August 1999), 290-294, doi: 10.1016/S0040-6090(99)00215-1.

Grätzel, M. (2001). Photoelectrochemical cells. *Nature,* 414, (November2001), 338-344, doi: 10.1038/35104607.

Grätzel, M. (2003). Dye-sensitized solar cells. *J. Photochem. Photobiol. C: Photochem. Rev.*, 4, (July 2003), 145-153, doi: 10.1016/S1389-5567(03)00026-1.

Gao, Y.; Nagai, M.; Chang, T.-C. & Shyue, J.-J. (2007). Solution-Derived ZnO Nanowire Array Film as Photoelectrode in Dye-Sensitized Solar Cells. *Crystal Growth & Design*, 7, 12, (November 2007), 2467-2471, DOI: 10.1021/cg060934k.

Grätzel, M. & Durrant, J.R. (2008). Dye-Sensitized Mesoscopic Solar Cells. In: *Nanostructured and photoelectrochemical systems for solar photon conversion*, Archer, M.D. & Nozik, A.J., 503-536, Imperial College Press Co., ISBN: 978-1-86094-255-6, London.

Gentilini, D ; D'Ercole, D.; Gagliardi, A.; Brunetti, A.; Reale, A.; Brown, T. &Di Carlo, A.(2010). Analysis and simulation of incident photon to current efficiency in dye sensitized solar cells. *Superlattices Microstruct.,* 47, 1, (January 2010), 192-196, doi:10.1016/j.spmi.2009.10.005.

Hara, K.; Sayama, K.; Ohga, Y.; Shinpo, A.; Suga ,S. & Arakawa, H. (2000). A coumarin-derivative dye sensitized nanocrystalline TiO_2 solar cell having a high solar-energy conversion efficiency up to 5.6%. *Chem. Commun.*, (March 2001), 569–570, DOI: 10.1039/b010058g.

Huber, R.; Spörlein, S.; Moser, J. E.; Grätzel, M. & Wachtveitl, J. (2000). The Role of Surface States in the Ultrafast Photoinduced Electron Transfer from Sensitizing Dye Molecules to Semiconductor Colloids. *J. Phys. Chem. B*, 104, 38, (September 2000), 8995-9003, DOI: 10.1021/jp9944381.

Hore, S.; Vetter, C.; Kern, R.; Smit, H.; Hinsch, A. (2006). Influence of scattering layers on efficiency of dye-sensitized solar cells. *Sol. Energy Mater. Sol. Cells,* 90, 9, (Mayb2006), 1176–1188, doi:10.1016/j.solmat.2005.07.002.

Hattori, R. & Goto, H. (2007). Carrier leakage blocking effect of high temperature sputtered TiO_2 film on dye-sensitized mesoporous photoelectrode. *Thin Solid Films*, 515, 20-21, (July 2007), 8045–8049, doi:10.1016/j.tsf.2007.03.079.

Hossain, M.F.; Biswas, S. & Takahashi, T. (2008). The effect of sputter-deposited TiO2 passivating layer on the performance of dye-sensitized solar cells based on sol–gel derived photoelectrode. *Thin Solid Films*, 517, 3, (December 2008), 1294–1300, doi:10.1016/j.tsf.2008.06.027.

Hod, I.; Shalom, M.; Tachan, Z., Rühle, S. & Zaban, A. (2010). $SrTiO_3$ Recombination-Inhibiting Barrier Layer for Type II Dye-Sensitized Solar Cells. *J. Phys. Chem. C*, 114, 21, (May 2010), 10015–10018, DOI: 10.1021/jp101097j.

Jung, H.S.; Lee, J.-K.; Nastasi, M.; Lee, S.-W.; Kim, J.-Y.; Park, J.-S.; Hong, K.S. & Shin, K. (2005). Preparation of Nanoporous MgO-Coated TiO_2 Nanoparticles and Their Application to the Electrode of Dye-Sensitized Solar Cells. *Langmuir*, 21, 23, (October 2005), 10332-10335, DOI: 10.1021/la051807d.

Jiang, C. Y.; Sun, X. W.; Lo, G. Q. & Kwong, D. L. (2007). Improved dye-sensitized solar cells with a ZnO-nanoflower photoanode. *Appl. Phys. Lett.*, 90, 26, (June 2007), 263501, doi:10.1063/1.2751588.

Jose, R.; Thavasi, V. & Ramakrishna, S. (2009). Metal Oxides for Dye-Sensitized Solar Cells. *J. Am. Ceram. Soc.*, 92, 2, (February 2009), 289–301, DOI: 10.1111/j.1551-2916.2008.02870.x.

Ko, K.H.; Lee, Y.C. & Jung, Y.J. (2005). Enhanced efficiency of dye-sensitized TiO_2 solar cells (DSSC) by doping of metal ions. *J. Colloid Interface Sci.*, 283, 2, (March 2005), 482–487, doi:10.1016/j.jcis.2004.09.009.

Ku, C.-H. & Wu, J.-J. (2007). Electron transport properties in ZnO nanowire array/nanoparticle composite dye-sensitized solar cells. *Appl. Phys. Lett.*, 91, 9, (August 2007), 093117, doi:10.1063/1.2778454.

Kang, S.H.; Choi, S.-H.; Kang, M.-S.; Kim, J.-Y.; Kim, H.-S.; Hyeon, T. & Sung, Y.-E. (2008). Nanorod-Based Dye-Sensitized Solar Cells with Improved Charge Collection Efficiency. *Adv. Mater.*, 20, 1, (January 2008), 54–58, DOI: 10.1002/adma.200701819.

Kim, Y.J.; Lee, Y.H.; Lee, M.H.; Kim, H.J.; Pan, J.H.; Lim, G.I.; Choi, Y.S.; Kim, K.; Park, N.-G.; Lee, C. & Lee, W.I. (2008). Formation of Efficient Dye-Sensitized Solar Cells by Introducing an Interfacial Layer of Long-Range Ordered Mesoporous TiO_2 Thin Film. *Langmuir*, 24, 22, (October 2008), 13225-13230, DOI: 10.1021/la802340g.

Li, B.; Wang, L.; Kang, B.; Wang, P. & Qiu, Y. (2006). Review of recent progress in solid-state dye-sensitized solar cells. *Sol. Energy Mater. Sol. Cells*, 90, 5, (March 2006), 549–573, doi:10.1016/j.solmat.2005.04.039.

Lotnyk, A.; Senz, S. & Hesse, D. (2007). Epitaxial growth of TiO_2 thin films on $SrTiO_3$, $LaAlO_3$ and yttria-stabilized zirconia substrates by electron beam evaporation. *Thin Solid Films*, 515, (December 2006), 3439–3447, doi:10.1016/j.tsf.2006.10.106.

Li, J.-G.; Ishigaki, T. & Sun, X. (2007). Anatase, Brookite, and Rutile Nanocrystals via Redox Reactions under Mild Hydrothermal Conditions: Phase-Selective Synthesis and Physicochemical Properties. *J. Phys. Chem. C*, 111, 13, (March 2007), 4969-4976, DOI: 10.1021/jp0673258.

Lee, S.; Kim, J.Y.; Youn, S.H.; Park, M.; Hong, K.S.; Jung, H.S.; Lee, J.-K. & Shin, H. (2007). Preparation of a Nanoporous $CaCO_3$-Coated TiO_2 Electrode and Its Application to a Dye-Sensitized Solar Cell. *Langmuir*, 23, 23, (October 2007), 11907-11910, DOI: 10.1021/la701826v.

Lee, S.; Noh, J.H.; Han, H.S.; Yim, D.K.; Kim, D.H.; Lee, J.-K.; Kim, J.Y.; Jung, H.S. & Hong, K.S. (2009). Nb-Doped TiO_2: A New Compact Layer Material for TiO_2 Dye-Sensitized Solar Cells. *J. Phys. Chem. C*, 113, 16, (March 2009), 6878–6882, DOI: 10.1021/jp9002017.

Lü, X.; Mou, X.; Wu, J.; Zhang, D.; Zhang, L.; Huang, F.; Xu, F. & Huang, S. (2010). Improved-Performance Dye-Sensitized Solar Cells Using Nb-Doped TiO_2 Electrodes: Efficient Electron Injection and Transfer. *Adv. Funct. Mater.*, 20, 3, (February 2010), 509–515, DOI: 10.1002/adfm.200901292.

Martinson, A. B. F.; Go´es, M. S.; Fabregat-Santiago, F.; Bisquert, J.; Pellin, M. J. &Hupp, J. T. (2009). Electron Transport in Dye-Sensitized Solar Cells Based on ZnO Nanotubes: Evidence for Highly Efficient Charge Collection and Exceptionally Rapid Dynamics. *J. Phys. Chem. A*, 113, 16, (February 2009), 4015–4021, DOI: 10.1021/jp810406q

Marco, L.D.; Manca, M.; Giannuzzi, R.; Malara, F.; Melcarne, G.; Ciccarella, G.; Zama, I.; Cingolani, R. & Gigli, G. (2010). Novel Preparation Method of TiO_2-Nanorod-Based Photoelectrodes for Dye-Sensitized Solar Cells with Improved Light-Harvesting Efficiency. *J. Phys. Chem. C*, 114, 9, (February 2010), 4228–4236, DOI: 10.1021/jp910346d.

Nusbaumer, H.; Moser, J. E.; Zakeeruddin, S. M.; Nazeeruddin, K. & Grätzel, M. (2001). $Co^{II}(dbbip)_2^{2+}$ Complex Rivals Tri-iodide/Iodide Redox Mediator in Dye-Sensitized Photovoltaic Cells. *J. Phys. Chem. B*, 105, 43, (October 2001), 10461-10464, DOI: 10.1021/jp012075a.

O'Regan, B. & Grätzel, M. (1991). A low-cost, high efficiency solar cell based on dye-sensitized colloidal TiO_2 films. *Nature,* 353, (October 1991), 737–740, doi: 10.1038/353737a0.

Pang, S.; Xie, T.; Zhang, Y.; Wei, X.; Yang, M. & Wang, D. (2007). Research on the Effect of Different Sizes of ZnO Nanorods on the Efficiency of TiO_2-Based Dye-Sensitized Solar Cells. *J. Phys. Chem. C*, 111, 49, (November 2007), 18417-18422, DOI: 10.1021/jp0763073.

Quintana, M.; Edvinsson, T.; Hagfeldt, A. & Boschloo, G. (2007). Comparison of Dye-Sensitized ZnO and TiO_2 Solar Cells: Studies of Charge Transport and Carrier Lifetime. *J. Phys. Chem. C,* 111, 2, (December 2006), 1035-1041, DOI: 10.1021/jp065948f.

Qian, J.; Liu, P.; Xiao, Y.; Jiang, Y.; Cao, Y.; Ai, X. & Yang, H. (2009). TiO_2-Coated Multilayered SnO_2 Hollow Microspheres for Dye-Sensitized Solar Cells. *Adv. Mater.*, 21, 36, (September 2009), 3663–3667, DOI: 10.1002/adma.200900525.

Redmond, G.; Fitzmaurice, D. & Gräetzel, M. (1994). Visible Light Sensitization by cis- Bis (thioc yanato) bis (2, 2'- bipyridyl-4, 4'-dicarboxylato) ruthenium (II) of a Transparent Nanocrystalline ZnO Film Prepared by Sol-Gel Techniques. *Chem. Mater.*, 6, 5, (May 1994), 686-691, DOI: 10.1021/cm00041a020.

Rengaraj, S.; Li, X.Z.; Tanner, P.A.; Pan, Z.F.; Pang, G.K.H. (2005). Photocatalytic degradation of methylparathion—An endocrine disruptor by Bi^{3+}-doped TiO_2. *J. Mol. Catal. A: Chem.,* 247, 1-2, (November 2005), 36–43, doi:10.1016/j.molcata.2005.11.030.

Rahman, M. M.; Ahammad, A. J. S.; Jin, J.-H.; Ahn, S. J. & Lee, J.-J. (2010). A Comprehensive Review of Glucose Biosensors Based on Nanostructured Metal-Oxides. *Sensors*, 10, 5, (May 2010), 4855-4886, doi:10.3390/s100504855.

Solbrand, A.; Keis, K.; Södergren, S.; Lindström, H.; Lindquist, S. E. & Hagfeldt, A. (2000). Charge transport properties in the nanostructured ZnO thin film electrode - electrolyte system studied with time resolved photocurrents. *Sol. Energy Mater. Sol. Cells*, 60, 2, (January 2000), 181-193, doi: 10.1016/S0927-0248(99)00083-5.

Sapp, S.A.; Elliott, M.; Contado, C.; Caramori, S. & Bignozzi, C.A. (2002). Substituted Polypyridine Complexes of Cobalt(II/III) as Efficient Electron-Transfer Mediators in Dye-Sensitized Solar Cells. *J. Am. Chem. Soc.*, 124, 37, (August 2002), 11215-11222, DOI: 10.1021/ja027355y.

Shin, K.; Jun, Y.; Moon, J.H. &Park, J.H. (2010). Observation of Positive Effects of Freestanding Scattering Film in Dye-Sensitized Solar Cells. *ACS Appl. Mater. Interfaces.*, 2, 1, (December 2009), 288-291, DOI: 10.1021/am900691c.

Tae, E. L.; Lee, S. H.; Lee, J. K.; Yoo, S. S.; Kang, E. J. & Yoon, K. B. (2005). A Strategy To Increase the Efficiency of the Dye-Sensitized TiO_2 Solar Cells Operated by Photoexcitation of Dye-to-TiO_2 Charge-Transfer Bands. *J. Phys. Chem. B,* 109, 47, (November 20005), 22513-22522, DOI: 10.1021/jp0537411.

Thavasi, V.; Renugopalakrishnan, V.; Jose, R. & Ramakrishna, S. (2009). Controlled electron injection and transport at materials interfaces in dye sensitized solar cells. *Mat. Sci. Eng. R,* 63, 3, (January 2009), 81–99, doi:10.1016/j.mser.2008.09.001

Umar, A. (2009). Growth of Comb-like ZnO Nanostructures for Dye-sensitized Solar Cells Applications. *Nanoscale Res Lett.,* 4, 9, (May 2009), 1004–1008, DOI: 10.1007/s11671-009-9353-3.

Umar, A.; Al-Hajry, A.; Hahn, Y.B. & Kim, D.H. (2009). Rapid synthesis and dye-sensitized solar cell applications of hexagonal-shaped ZnO nanorods. *Electrochim. Acta*, 54, 23, (September 2009) 5358–5362, doi:10.1016/j.electacta.2009.04.015.

Wang, Z.-S.; Huang, C.-H.; Huang, Y.-Y.; Hou, Y.-J.; Xie, P.-H.; Zhang, B.-W. & Cheng, H.-M. (2001). A Highly Efficient Solar Cell Made from a Dye-Modified ZnO-Covered TiO_2 Nanoporous Electrode. *Chem. Mater.*, 13, 2, (January 2001), 678-682, DOI: 10.1021/cm000230c.

Wang, Y.; Hang, K.; Anderson, N. A.; Lian, T. (2003). Comparison of Electron Transfer Dynamics in Molecule-to-Nanoparticle and Intramolecular Charge Transfer Complexes. *J. Phys. Chem. B,* 107, 35, (July 2003), 9434-9440, DOI: 10.1021/jp034935o.

Wang, P; Zakeeruddin, S.K.; Moser, J-E.; Humphry-Baker, R. & Grätzel, M. (2004). A Solvent-Free, SeCN-/$(SeCN)^3$- Based Ionic Liquid Electrolyte for High-Efficiency Dye-Sensitized Nanocrystalline Solar Cells. *J. Am. Chem. Soc.,* 126, 23, (May 2004), 7164-7165, DOI: 10.1021/ja048472r.

Wang, P.; Dai, Q.; Zakeeruddin, S.M.; Forsyth, M.; MacFarlane, D.R. & Grätzel, M. (2004). Ambient Temperature Plastic Crystal Electrolyte for Efficient, All-Solid-State Dye-Sensitized Solar Cell. *J. Am. Chem. Soc.*, 126, 42, (October 2004), 13590-13591, DOI: 10.1021/ja045013h.

Wang, H.; Li, H.; Xue, B.; Wang, Z.; Meng, Q. & Chen, L. (2005). Solid-State Composite Electrolyte LiI/3-Hydroxypropionitrile/SiO_2 for Dye-Sensitized Solar Cells. *J. Am. Chem. Soc.,* 127, 17, (April 2005), 6394-6401, DOI: 10.1021/ja043268p.

Wei, M.; Qi, Z.-M.; Ichihara, M. & Zhou, H. (2008). Synthesis of single-crystal niobium pentoxide nanobelts. *Acta Materialia*, 56, 11, (June 2008), 2488–2494, doi:10.1016/j.actamat.2008.01.049.

Wu, J.; Lan, Z.; Hao, S.; Li, P.; Lin, J.; Huang, M.; Fang, L. & Huang, Y. (2008). Progress on the electrolytes for dye-sensitized solar cells. *Pure Appl. Chem.*, 80, 11, (November 2008), 2241–2258, doi: 10.1351/pac200880112241.

Wang, H.; Liu, Y.; Li, M.; Huang, H.; Zhong, M. & Shen, H. (2009). Hydrothermal growth of large-scale macroporous TiO_2 nanowires and its application in 3D dye-sensitized solar cells. *Appl. Phys. A*, 97, 1, (August 2009), 25–29, DOI: 10.1007/s00339-009-5369-x.

Wang, J.X.; Wu, C. M. L. ; Cheung, W. S.; Luo, L. B.; He, Z. B.; Yuan, G. D.; Zhang, W. J.; Lee, C. S. & Lee, S. T. (2010). Synthesis of Hierarchical Porous ZnO Disklike Nanostructures for Improved Photovoltaic Properties of Dye-Sensitized Solar Cells. *J. Phys. Chem. C,* 114, 31, (July 2010), 13157–13161, DOI: 10.1021/jp100637c.

Xu, F.; Dai, M.; Lu, Y. & Sun, L. (2010). Hierarchical ZnO Nanowire-Nanosheet Architectures for High Power Conversion Efficiency in Dye-Sensitized Solar Cells. *J. Phys. Chem. C,* 114, 6, (January 2010), 2776–2782, DOI: 10.1021/jp910363w.

Yum, J.-H.; Nakade, S.; Kim, D.-Y. & Yanagida, S. (2006). Improved Performance in Dye-Sensitized Solar Cells Employing TiO_2 Photoelectrodes Coated with Metal Hydroxides. *J. Phys. Chem. B,* 110, 7, (February 2006), 3215-3219, DOI: 10.1021/jp0564593.

Yao, Q.; Liu, J.; Peng, Q.; Wang, X. & Li, Y. (2006). Nd-Doped TiO_2 Nanorods: Preparation and Application in Dye-Sensitized Solar Cells. *Chem. Asian J.*, 1, 5, 737 – 741, DOI: 10.1002/asia.200600195.

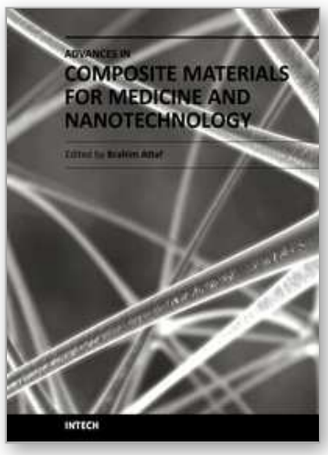
Yu, H.; Zhang, S.; Zhao, H.; Will, G. & Liu, P. (2009). An efficient and low-cost TiO_2 compact layer for performance improvement of dye-sensitized solar cells. *Electrochim. Acta*, 54, 4, (January 2009), 1319–1324, doi:10.1016/j.electacta.2008.09.025.

Yi, Z.M.; Hai, W.; Yong, L.; Ming, L.; Hong, H. & Hui, S. (2010). ZnO microsheet modified TiO_2 nanoparticle composite films for dye-sensitized solar cells. *Chinese Sci. Bul.*, 55, 18, (June 2010), 1945-1948, DOI: 10.1007/s11434-009-3688-0.

Zhu, K.; Neale, N. R.; Miedaner, A. & Frank, A. J. (2006). Enhanced Charge-Collection Efficiencies and Light Scattering in Dye-Sensitized Solar Cells Using Oriented TiO_2 Nanotubes Arrays. *Nano Lett.,* 7, 1, (December 2006), 69-74, DOI: 10.1021/nl062000o.

Zhu, K.; Vinzant, T. B.; Neale, N. R. & Frank, A. J. (2007). Removing Structural Disorder from Oriented TiO_2 Nanotube Arrays: Reducing the Dimensionality of Transport and Recombination in Dye-Sensitized Solar Cells. *Nano Lett.*, 7, 12, (November 2007), 3739-3746, DOI: 10.1021/nl072145a.

Zhang, W.; Zhu, R.; Liu, X.; Liu, B. & Ramakrishna, S. (2009). Facile construction of nanofibrous ZnO photoelectrode for dye-sensitized solar cell applications, *Appl. Phys. Lett.,* 95, 4, (July 2009), 043304, doi:10.1063/1.3193661.



Advances in Composite Materials for Medicine and Nanotechnology

Edited by Dr. Brahim Attaf

ISBN 978-953-307-235-7
Hard cover, 648 pages
Publisher InTech
Published online 01, April, 2011
Published in print edition April, 2011

Due to their good mechanical characteristics in terms of stiffness and strength coupled with mass-saving advantage and other attractive physico-chemical properties, composite materials are successfully used in medicine and nanotechnology fields. To this end, the chapters composing the book have been divided into the following sections: medicine, dental and pharmaceutical applications; nanocomposites for energy efficiency; characterization and fabrication, all of which provide an invaluable overview of this fascinating subject area. The book presents, in addition, some studies carried out in orthopedic and stomatological applications and others aiming to design and produce new devices using the latest advances in nanotechnology. This wide variety of theoretical, numerical and experimental results can help specialists involved in these disciplines to enhance competitiveness and innovation.

How to reference

In order to correctly reference this scholarly work, feel free to copy and paste the following:

Jae-Joon Lee, Md. Mahbubur Rahman, Subrata Sarker, N.C. Deb Nath, A.J. Saleh Ahammad and Jae Kwan Lee (2011). Metal Oxides and Their Composites for the Photoelectrode of Dye Sensitized Solar Cells, Advances in Composite Materials for Medicine and Nanotechnology, Dr. Brahim Attaf (Ed.), ISBN: 978-953-307-235-7, InTech, Available from: http://www.intechopen.com/books/advances-in-composite-materials-for-medicine-and-nanotechnology/metal-oxides-and-their-composites-for-the-photoelectrode-of-dye-sensitized-solar-cells

INTECH
open science | open minds

InTech Europe
University Campus STeP Ri
Slavka Krautzeka 83/A
51000 Rijeka, Croatia
Phone: +385 (51) 770 447
Fax: +385 (51) 686 166
www.intechopen.com

InTech China
Unit 405, Office Block, Hotel Equatorial Shanghai
No.65, Yan An Road (West), Shanghai, 200040, China
中国上海市延安西路65号上海国际贵都大饭店办公楼405单元
Phone: +86-21-62489820
Fax: +86-21-62489821

© 2011 The Author(s). Licensee IntechOpen. This chapter is distributed under the terms of the Creative Commons Attribution-NonCommercial-ShareAlike-3.0 License, which permits use, distribution and reproduction for non-commercial purposes, provided the original is properly cited and derivative works building on this content are distributed under the same license.

IntechOpen

IntechOpen